Concurrent MORB-type and ultrapotassic volcanism in an extensional basin along the Laurentian Iapetus margin: Tectonomagmatic response to Ordovician arc-continent collision and subduction polarity flip

Deta Gasser[1,2,†], Tor Grenne[2], Fernando Corfu[3], Reidulv Bøe[2], Torkil S. Røhr[2], and Trond Slagstad[2]

[1]*Department of Environmental Sciences, Western Norway University of Applied Sciences, Røyrgata 6, 6856 Sogndal, Norway*
[2]*Geological Survey of Norway, PO Box 6315, Torgarden, 7491 Trondheim, Norway*
[3]*Department of Geosciences and CEED, University of Oslo, PO Box 1047, Blindern, 0316 Oslo, Norway*

ABSTRACT

Arc-continent collision, followed by subduction polarity flip, occurs during closure of oceanic basins and contributes to the growth of continental crust. Such a setting may lead to a highly unusual association of ultrapotassic and mid-ocean ridge basalt (MORB)-type volcanic rocks as documented here from an Ordovician succession of the Scandinavian Caledonides. Interbedded with deep-marine turbidites, pillow basalts evolve from depleted-MORB (εNd_t 9.4) to enriched-MORB (εNd_t 4.8) stratigraphically upward, reflecting increasingly deeper melting of asthenospheric mantle. Intercalated intermediate to felsic lava and pyroclastic units, dated at ca. 474–469 Ma, are extremely enriched in incompatible trace elements (e.g., Th) and have low εNd_t (−8.0 to −6.6) and high Sr_i (0.7089–0.7175). These are interpreted as ultrapotassic magmas derived from lithospheric mantle domains metasomatized by late Paleoproterozoic to Neoproterozoic crust-derived material (isotopic model ages 1.7–1.3 Ga). Detrital zircon spectra reveal a composite source for the interbedded turbidites, including Archean, Paleo-, to Neoproterozoic, and Cambro-Ordovician elements; clasts of Hølonda Porphyrite provide a link to the Hølonda terrane of Laurentian affinity. The entire volcano-sedimentary succession is interpreted to have formed in a rift basin that opened along the Laurentian margin as a result of slab rollback subsequent to arc-continent collision, ophiolite obduction and subduction polarity flip. The association of MORBs and ultrapotassic rocks is apparently a unique feature along the Caledonian-Appalachian orogen. Near-analogous modern settings include northern Taiwan and the Tyrrhenian region of the Mediterranean, but other examples of strictly concurrent MORB and ultrapotassic volcanism remain to be documented.

INTRODUCTION

Ophiolites, island arcs and associated sedimentary basins are preserved in many ancient orogens, playing a crucial role in identifying oceanic sutures and reconstructing the opening and closure history of ancient oceanic basins (e.g., Burke et al., 1977). Arc-continent collisions, often associated with a subsequent subduction polarity flip, play a major role in the closure history of such oceanic basins and contribute to the growth of the continental crust (Clift et al., 2003, 2004; Dewey, 2005; Brown et al., 2011).

One of the major orogenic belts in which continental collision was preceded by arc-continent collision(s) is the Caledonian-Appalachian orogen of the North Atlantic region (Fig. 1). Based on the presence of widely different faunas of similar age juxtaposed against each other, Wilson (1966) proposed the existence of a Paleozoic "proto-Atlantic" ocean, later termed Iapetus (Harland and Gayer, 1972). A variety of ophiolites, island-arcs and related sedimentary basins has been described all along the orogen, recounting a complex story of Cambrian to Silurian intra-oceanic subduction, arc-continent collision, opening of marginal basins and subduction polarity flips prior to the ultimate collision between Laurentia, Baltica, and Gondwana-derived terranes (Fig. 1; Pedersen et al., 1992; van Staal et al., 2009; Zagorevski and van Staal, 2011; Cooper et al., 2011; Ryan and Dewey, 2011; Furnes et al., 2012; Hollis et al., 2012; Slagstad et al., 2014).

The Trondheim Nappe Complex (Fig. 2A) of the Central Scandinavian Caledonides, with its well-preserved ophiolite fragments (Grenne et al., 1999; Slagstad et al., 2014) and rich fossil faunas of both Laurentian, intra-Iapetus (Celtic) and Baltic affiliation (Bruton and Bockelie, 1980; Gee, 1981; Harper et al., 1996) has long been a crucial area for reconstructing the history of Iapetus. Specifically, the unequivocal Laurentian faunal affinity of shales and limestones in the Hølonda terrane is widely accepted as a paleogeographic marker for the Løkken-Vassfjellet-Bymarka (LVB) ophiolite and its overlying Early- to Mid-Ordovician strata (Fig. 2A; Bruton and Bockelie, 1980; Neuman and Bruton, 1989; Harper et al., 1996).

The LVB ophiolite is generally interpreted as having been obducted onto the Laurentian margin or an associated microcontinent shortly after its formation in the Late Cambrian to Early Ordovician, followed by a shift in subduction polarity from southeast- to northwest-vergent and onset of continental-arc magmatism in Mid-Ordovician times, the latter represented by the Hølonda Porphyrites (Fig. 2B; Grenne and Roberts, 1998; Slagstad et al., 2014). This proposed scenario is similar to the Grampian and Taconian arc-continent collision and associated subduction polarity flip known from the Irish and Newfoundland sectors of the Caledonian-Appalachian orogen (Cooper et al., 2011; Ryan and Dewey, 2011; Zagorevski and van Staal, 2011). In the Norwegian sector, however, the details of this process are not well understood, and the genesis and tectonic significance of several volcano-sedimentary units adjacent to the LVB ophiolite are unknown.

In this contribution, we present stratigraphic, geochemical, isotopic, and geochronological data from a volcano-sedimentary succession adjacent to the LVB ophiolite. This succession, here referred to as the Ilfjellet Group (Figs. 2A

Deta Gasser https://orcid.org/0000-0001-7300-8984
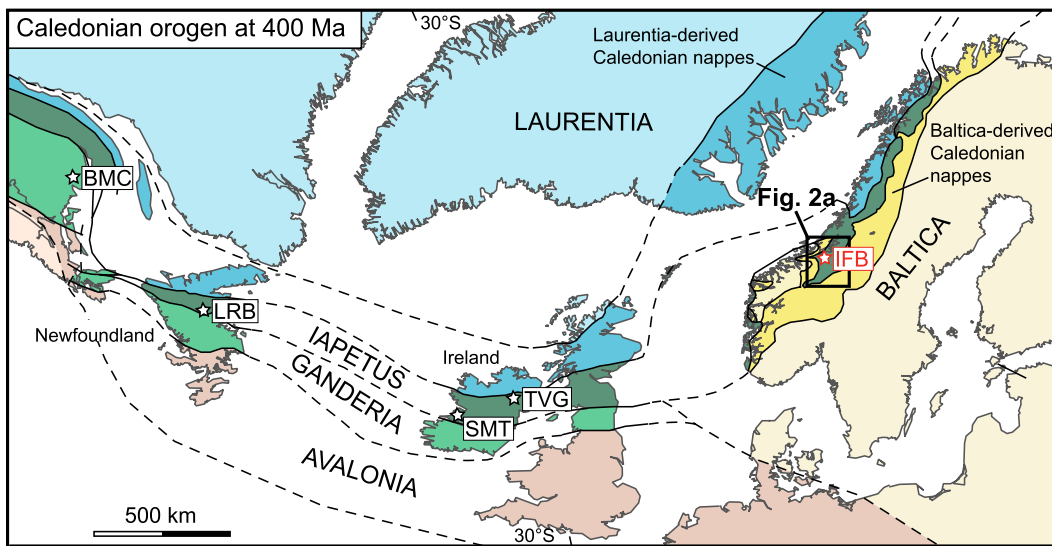
†deta.gasser@hvl.no.

Figure 1. The Caledonian orogen reconstructed at 400 Ma after Domeier (2016). Ophiolites, island arcs, and sedimentary basins from the Iapetus Ocean are preserved along a narrow belt from the Scandinavian Caledonides through the British Isles to Newfoundland, Canada. Abbreviations for 475–470 Ma volcanosedimentary units discussed in the text: BMC—Bathurst Mining Camp; IFB—Ilfjellet basin; LRB—Lloyds River basin; TVG—Tyrone Volcanic Group; SMT—South Mayo Trough.

and 2B), contains a peculiar association of mid-ocean ridge basalts (MORB) and highly enriched, predominantly intermediate volcanic rocks that is apparently unique in the Caledonian-Appalachian orogen. We discuss the formation of this basin within the framework of arc-continent collision and subsequent subduction polarity reversal and compare it with possible modern tectonic analogues.

GEOLOGICAL BACKGROUND

The Trondheim Nappe Complex is preserved within a large-scale NNE-SSW–trending synform in central Norway (Fig. 2A; Roberts and Wolff, 1981; Gee et al., 1985). Three major, predominantly basaltic, greenschist facies metavolcanic belts occur here: the LVB ophiolite to the northwest, a central belt stretching from Oppdal to Mostadmarka that includes the Ilfjellet Group, and the eastern Fundsjø Group running through Meråker (Fig. 2A). Low-grade metasedimentary rocks of the Hovin and Horg groups are exposed between the western and central belts, whereas generally higher-grade metasedimentary, volcanic, and intrusive rocks of the Gula Complex separate the central and eastern belts (Fig. 2A; Wolff, 1979; Gee et al., 1985).

Both the LVB ophiolite and the central metavolcanic belt have traditionally been referred to as the Støren Group (e.g., Kjerulf, 1883; Wolff, 1979; Gee et al., 1985; Slagstad et al., 2014). Of these, the LVB ophiolite is so far best studied, particularly at Løkken and Vassfjellet (Fig. 2B) where a thick succession of pillow lava is underlain by sheeted dikes and gabbros with comagmatic plagiogranite (Grenne et al., 1980; Heim et al., 1987; Grenne, 1980, 1989). Geochemically, the ophiolite shows supra-sub-

duction zone signatures and is interpreted to have formed in an oceanic back-arc marginal basin (Grenne et al., 1999; Slagstad, 2003; Furnes et al., 2014; Slagstad et al., 2014), associated with an island arc represented by the Gjersvik Group farther north (Grenne et al., 1999). U-Pb dates of plagiogranites indicate that the LVB ophiolite formed between 487 and 480 Ma (Roberts et al., 2002; Slagstad et al., 2014).

Several authors have noted a lithological difference between the LVB ophiolite and the central metavolcanic belt extending through the town of Støren (Fig. 2B), the latter lacking gabbro and sheeted dike complexes but containing distinct ribbon chert (Grenne et al., 1999). This metavolcanic belt has therefore been referred to by some authors as Støren Group sensu stricto (s.s.) (Grenne et al., 1999; Stokke et al., 2018). It has been speculated that the Støren Group s.s. is older than the LVB ophiolite (Furnes et al., 1980, 1985; Roberts et al., 1984, 1985; Sturt et al., 1984), but modern geochemical data and U-Pb dates of magmatic rocks have been lacking.

Southeast of Trondheim, the minor Jonsvatnet Greenstone Formation (Grenne and Roberts, 1983), lithologically comparable to the Støren Group s.s., is separated from the LVB ophiolite by a metasedimentary succession referred to here as the Klæbu Formation (Fig. 2B). These metasediments were assigned to the Hovin Group in a regional map compilation by Wolff (1976), but it is unclear from Wolff's map whether the Jonsvatnet basalts were interpreted as an integral part of the younger Hovin Group, or if the basalts represent tectonic slivers of either the LVB ophiolite or the Støren Group s.s.

Metabasaltic rocks in the Oppdal area (Fig. 2A) were interpreted by Nilsen and Wolff (1989) as a southward continuation of the

Støren Group s.s. This Trollhøtta unit comprises MORBs geochemically distinct from the LVB ophiolites (Stokke et al., 2018; Dalslåen et al., 2020a) and is coeval with highly enriched volcanic rocks of the Kinna volcanic succession and the Storgruvpiken rhyolite (Fig. 2A) dated at ca. 475–470 Ma (Dalslåen et al., 2020b).

→

Figure 2. (A) Simplified geological map of the Trondheim Nappe Complex, central Scandinavian Caledonides. Geographic abbreviations: H—Hølonda; M—Mostadmarka; Me—Meråker; O—Oppdal; T—Trondheim. *The lower part of the Ilfjellet Group (Mostadmarka Formation, Fig. 2B) has traditionally been referred to as the Støren Group s.s. (B) Geological map showing our new stratigraphic interpretation of the western Trondheim Nappe Complex and the location of samples analyzed for geochemistry and geochronology. Note that the Klæbu, Fjellvollen, and Føssjøen formations were previously interpreted as part of the Hovin Group. (C) Geological map of the Ilfjellet area, showing our new stratigraphic interpretation and the location of samples analyzed for geochemistry and geochronology. Note that brownish colors represent metabasaltic units, whereas greenish and bluish colors represent metasedimentary units, in accordance with color schemes for Norwegian bedrock maps (Gjelle and Sigmond, 1995). LVB—Løkken-Vassfjellet-Bymarka ophiolite; undiff.—undifferentiated; Fm—Formation; E-MORB—enriched-mid-ocean ridge basalt; T-MORB—transitional-mid-ocean ridge basalt; D-MORB—depleted-mid-ocean ridge basalt; s.s.—sensu stricto.
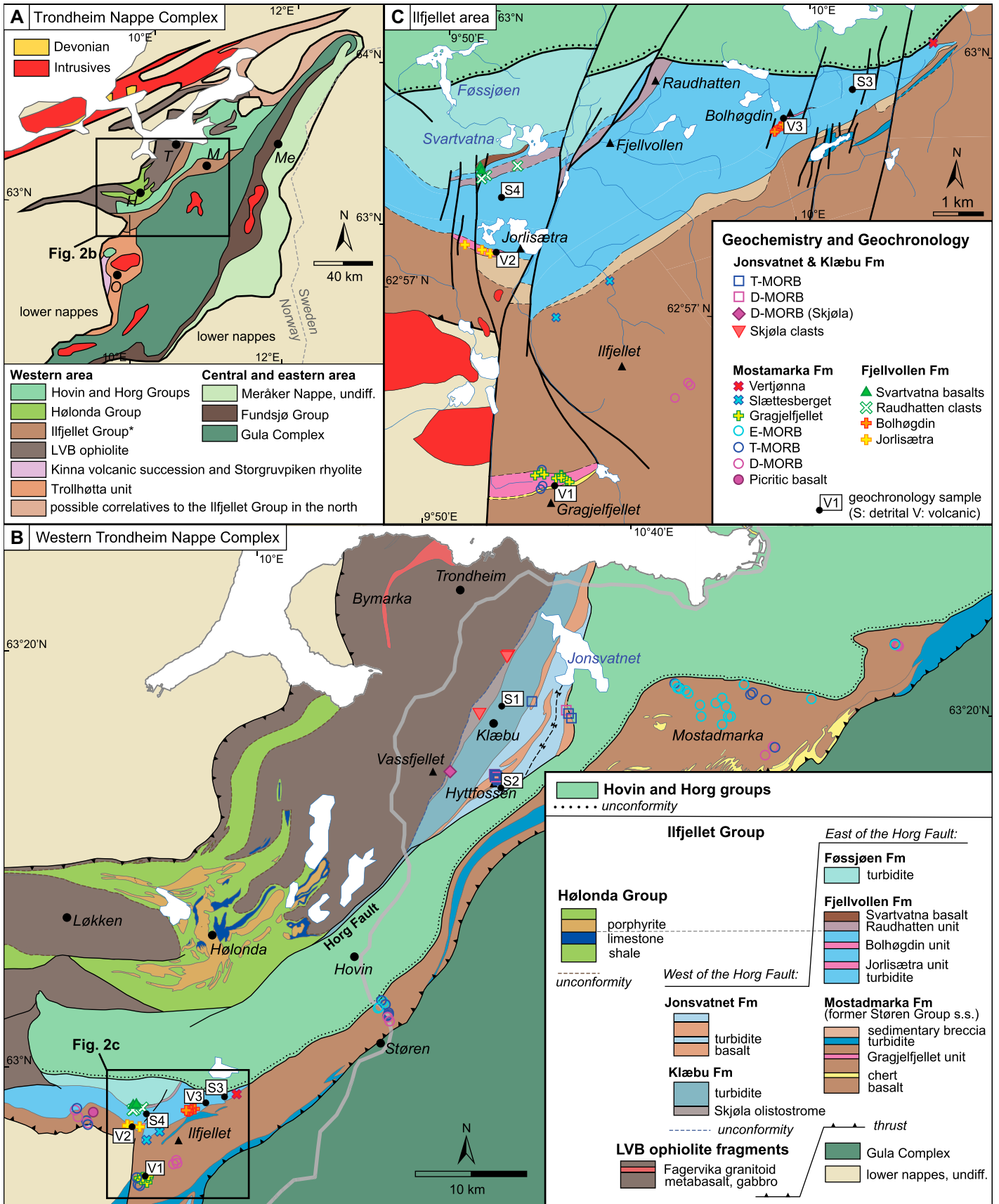
LITHOSTRATIGRAPHY

We investigated the basaltic rocks that have been referred to as the Støren Group s.s., and associated sedimentary successions, from the well-exposed mountainous area of Ilfjellet in the south to Mostadmarka in the north (Fig. 2B). In addition, we studied the Jonsvatnet Greenstone Formation and the under- and overlying sedimentary successions in the area east of Vassfjellet (Fig. 2B).

Based on our field observations, together with geochemical and geochronological data presented below, we suggest the following new stratigraphic terminology for the area (Figs. 2 and 3): The sedimentary Klæbu Formation unconformably overlies the LVB ophiolite and is in turn overlain by the basalt-dominated Jonsvatnet Formation. The Jonsvatnet Formation is correlated with the Mostadmarka Formation (former Støren Group s.s.), which is overlain by the sediment-dominated Fjellvollen and Føssjøen formations. All these units together constitute the Ilfjellet Group.

Klæbu Formation

At its base, the Klæbu Formation comprises the coarse conglomeratic Skjøla olistostrome (Grenne et al., 1980), which overlies the Vassfjellet ophiolite with a marked angular unconformity (Figs. 2B and 3A). It rests partly on pillow lavas and partly on the ophiolitic gabbro and sheeted dike complex. The true thickness of the olistostrome is estimated at up to l.2 km. Clast size is highly variable and locally up to 2–3 m. The matrix-supported lithology comprises angular to subrounded fragments of intermediate to felsic plutonic rocks, gabbro, pillow lava, jasper, diabase, and marble (Fig. 4A). Parts of the unit are dominated by quartz dioritic clasts that are compositionally similar to the Fagervika granitoid (Supplemental information, Fig. S1; Table S1[1]), which intruded the LVB ophiolites at 481 ± 3 Ma (Fig. 2B; Slagstad et al., 2014). One quartz dioritic clast has yielded a U-Pb thermal ionization mass spectrometry (TIMS) zircon age of 478 ± 1 Ma (Fig. S2; Table S2; see footnote 1), which is slightly younger but within error of the Fagervika pluton. Units 20–50 m thick of non-vesicular pillow basalt occur sporadically (Fig. 3A).

A siliciclastic succession, ∼3 km thick, overlies the Skjøla olistostrome (Figs. 2B and 3A). Lower parts are dominated by thin-bedded (typically cm-scale) siltstone and shale with minor sandy beds generally <10 cm thick (Fig. 4B). Grading, planar lamination and cross lamination are common and together with laterally persistent bedding point to a turbiditic origin. Silt- and sandstone beds are dominated by detrital quartz in a carbonate-rich matrix. Middle and upper parts of the Klæbu Formation show a gradual transition to thicker-bedded turbidites with up to meter-thick beds of variably quartz- or feldspar-rich sandstone (graywacke) and siltstone. Local granule and pebbly conglomerates contain clasts of quartz, feldspathic rocks, greenstone, and carbonate.

Jonsvatnet Formation

The Klæbu Formation is conformably overlain to the southeast by a ∼2-km-thick succession of basaltic and sedimentary rocks (Figs. 2B and 3A). The basaltic parts form laterally discontinuous units of non-vesicular or slightly vesicular (<1%) pillow lavas (Fig. 4C) and sheet flows with interbedded ribbon chert (Fig. 4D), siltstone, and cherty siltstone. Beds of oxide-facies iron formation and jasper (hematitic chert) occur locally. Clastic sedimentary parts of the Jonsvatnet Formation are similar to the underlying Klæbu Formation.

Mostadmarka Formation

The Mostadmarka Formation is in tectonic contact with the Gula Complex to the southeast (Figs. 2B and 3B). In the Ilfjellet-Støren area, where folding is limited, the true thickness of the Mostadmarka Formation is at least 2.1–5.2 km. Basaltic pillow lavas predominate (Figs. 3B and 5A) and locally alternate with sheet flows. Basalt vesicularity is <1% in the lower to middle parts of the formation; slightly vesicular (up to ∼5%) varieties occur only in the upper parts. Aphyric basalts predominate, but highly plagioclase-phyric lavas occur in the upper parts of the volcanic succession. Basaltic dikes appear sporadically at all stratigraphic levels.

Sulfide-, oxide-, and silicate-facies iron formation (Grenne and Slack, 2019) forms discrete units up to a few meters thick at various stratigraphic levels (Fig. 3B). Sulfidic varieties predominate at lower levels, comprising thin beds (mostly <1 cm) of pyrite or pyrrhotite, which are locally highly graphitic. At middle and upper levels, oxide-facies (magnetite and/or hematite) iron formation predominates. Beds of jasper, typically 1–5 m thick, also occur at middle and upper levels.

Units of ribbon chert, up to a few tens of meters in thickness, occur sparsely throughout the Mostadmarka Formation (Fig. 3B). In the middle and upper parts of the formation, the cherts show transitions into cherty siltstone and purely clastic, thin-bedded siltstone and fine-grained sandstone (Fig. 5B). The clastic sedimentary rocks are characterized by laterally persistent beds interpreted as distal turbidites, partly including complete Bouma sequences.

Sedimentary breccias with a thickness of several tens of meters and locally up to 300 m, in places with internal thin pillow lavas, are interbedded with lavas in middle and upper parts of the succession (Fig. 3B). In contrast to common flow-related pillow breccias, which are compositionally homogeneous and contain only pillow fragments in a hyaloclastite matrix, these thick sedimentary breccias contain basaltic clasts with different compositions and textures, locally including slightly vesicular (up to ∼5%) varieties, together with rare clasts of jasper, white chert, calcareous sandstone, and limestone, set in a calcareous matrix of mostly fine-grained basaltic debris (Fig. 5C). The clasts are typically 5–20 cm across and locally up to 1 m, generally with angular shapes or partly curved surfaces from the rims of broken pillows. The breccias are mostly unsorted; gritty to sandy interbeds occur locally (Fig. 5D).

Felsic or intermediate volcanic rocks are rare and were previously not reported from the Mostadmarka Formation. The most significant occurrence is the up to 200-m-thick and laterally restricted Gragjelfjellet unit (Figs. 2C and 3B). The unit overlies a ∼50-m-thick sedimentary unit comprising—from bottom to top—jasper, ribbon chert, and a thin-bedded, fine-grained greenish sandstone (Fig. 3B). The lower 25–30 m of the Gragjelfjellet unit is a felsic pyroclastic breccia comprising welded lapilli tuff in the lower half (Fig. 5E) and unwelded lapilli and bombs or blocks up to 70 × 30 cm in the upper parts. The pyroclastic breccia is overlain by an up to 50-m-thick felsic lava with ∼30% vesicularity at the top. The remaining upper 100–120 m of the Gragjelfjellet unit comprise felsic pyroclastic deposits and intermediate to mafic, massive or pillowed flows that are locally highly vesicular (Fig. 5F). Primary mineralogy in the Gragjelfjellet unit is largely obliterated by greenschist-facies regional metamorphism, but K-feldspar phenocrysts are abundant in felsic units and variably chloritized phlogopite or biotite is common in intermediate to mafic varieties.

In the uppermost part of the Mostadmarka Formation, the 50-m-thick Slættesberget unit (Figs. 2C and 3B) consists of highly vesicular (up to ∼50%; Fig. 5G) pillow lavas resting directly on ∼20 m of ribbon chert (Fig. 5H).
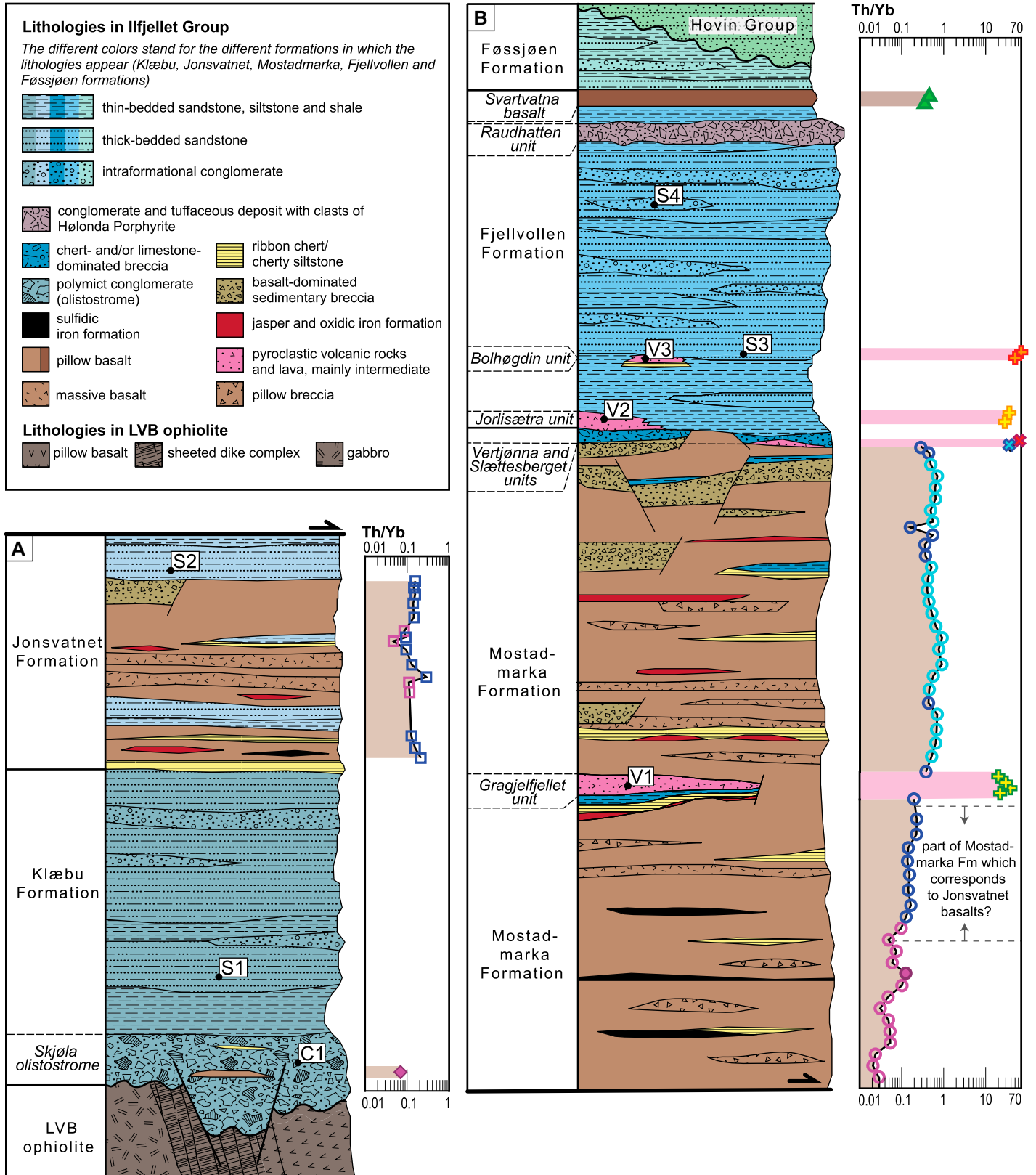
Figure 3. Schematic stratigraphic columns for (A) the Vassfjellet-Jonsvatnet area and (B) the Ilfjellet-Føssjøen area. For sample locations, see Figures 2B and 2C. The stratigraphic position of geochemistry and geochronology samples is indicated schematically. LVB—Løkken-Vassfjellet-Bymarka ophiolite; Fm—Formation.
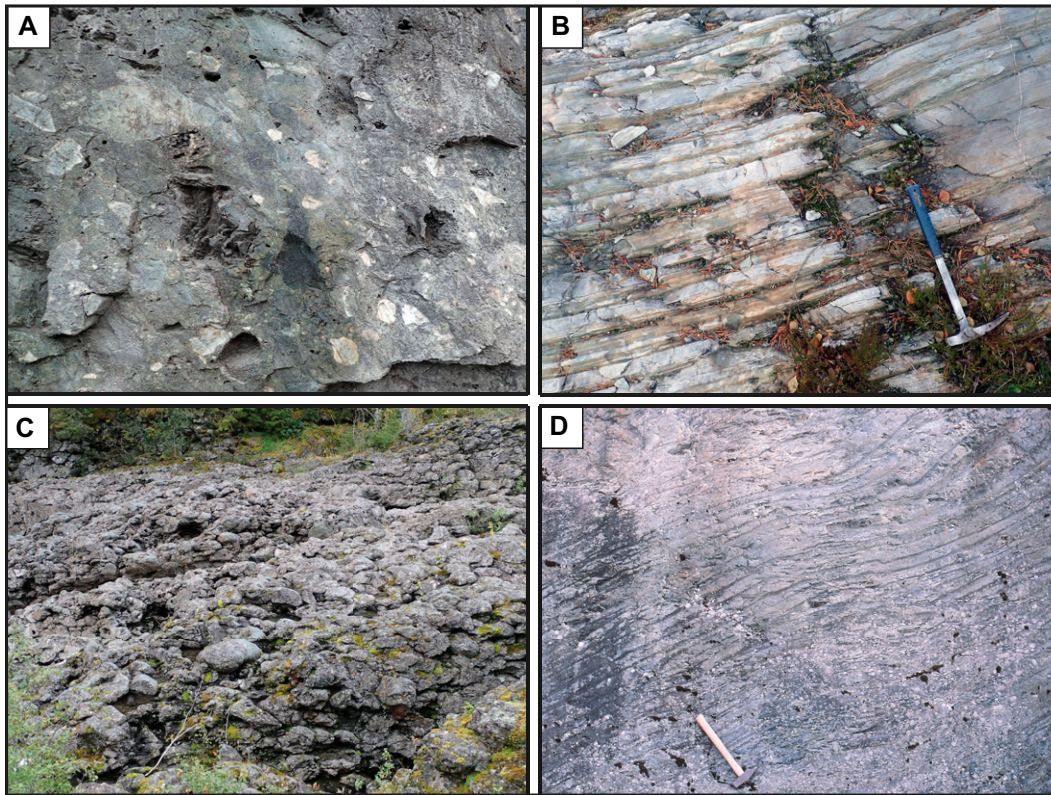
Figure 4. Field photographs from the Klæbu (A–B) and Jonsvatnet formations (C–D) (Fig. 2B). (A) Conglomeratic part of the Skjøla olistostrome with clasts of felsic magmatic rocks, metabasalt and limestone (weathered out) in a greenish matrix; width of photo ~70 cm (location coordinates: E571262/N7021356; coordinate system WGS84 UTM Zone 32N, here and for the following locations). (B) Relatively thin-bedded silt- and sandstone in the Klæbu Formation (E567882/N7011609). (C) Pillow lavas from the Jonsvatnet Formation at Hyttfossen, width of photo in the foreground is ~10 m (E573430/N7015330). Drained pillows are common, typically with internal lava shelves formed by the successive tapping of magma from pillow tubes on an inclined seafloor surface or along steep flowfronts. (D) Light-gray ribbon chert from the lower part of the Jonsvatnet Formation (E573279/N7016414).

Along strike and ~8 km to the northeast, the Vertjønna unit (Figs. 2C and 3B) comprises rhyolitic pyroclastic deposits, with fine-grained, non-vesicular clasts scattered in a compositionally similar matrix.

The top of the Mostadmarka Formation and the transition into the overlying Fjellvollen Formation is dominated by chaotic sedimentary breccias that include thin beds and large rafts (up to 7 × 1 m) of ribbon chert with widespread soft-sediment deformation as well as rafts and blocks of limestone, basalt, jasper, and chert.

Fjellvollen Formation

The predominantly siliciclastic Fjellvollen Formation has a maximum preserved thickness of ~2.3 km (Figs. 2B and 2C). Its lower 200–500 m comprises mainly distal turbidites, including thin-bedded (typically cm-scale) grayish or greenish-gray, quartz-rich siltstone and shale with minor sandstone beds. Northwest of Ilfjellet, however, the chaotic sedimentary breccias of the Mostadmarka Formation are overlain by the volcanic, 100-m-thick Jorlisætra unit (Figs. 2C and 3B). Here, units of lapilli tuff, at least 5 m thick, contain <5 cm (locally up to 10 cm) angular to subangular, variably vesicular clasts of a very fine-grained, light-gray felsic volcanic rock and minor epiclastic material in

a fine-grained felsic volcanic matrix (Fig. 5I). These units alternate with massive, fine-grained (<1 mm) tuff beds more than 8 m thick, locally interbedded with ribbon chert.

Stratigraphically above, within thin- to medium-bedded silt- and sandstones, the volcanic Bolhøgdin unit rests on local limestone and ribbon chert (Figs. 2C and 3B). The unit has a

Figure 5. Field photographs of the Mostadmarka (A–H) and Fjellvollen (I–O) formations (Fig. 2B). (A) Thin-rimmed pillow lava in upper part of the Mostadmarka Formation (E588814/N7025463). (B) Thin bed of light-purplish sandstone grading (up in photo) into grayish-green siltstone and shale with thin planar lamination (E551265/N6983994). (C) Sedimentary breccia dominated by basaltic angular clasts with subordinate limestone clasts in a calcareous matrix (E549324/N6983125). (D) Sedimentary breccia similar to that in C, with greenish sandstone layer dominated by basaltic detritus (E549355/N6983029). (E) Welded lapilli tuff at the base of the Gragjelfjellet volcanic unit; width of picture ~20 cm (E545519/N6976948). (F) Highly vesicular lava in the Gragjelfjellet unit; width of picture ~6 cm (E545010/N6977101). (G) Vesicular pillow lava of the Slættesberget unit, near the top of Mostadmarka Formation (E546230/N6981237). (H) Ribbon chert with highly distorted bedding related to soft-sediment deformation, near the top of Mostadmarka Formation (E545182/N6980383). (I) Lapilli tuff of the Jorlisætra unit. (J) Bolhøgdin volcanic unit; limestone (brown surfaces) densely veined by lava (gray) from overlying flow. Note peperitic mixing in intermediate gray-brown areas (e.g., lower left and upper parts of photo, above hand lens). Hand lens is ~3 cm (E549849/N6984132). (K) Contact between highly vesicular lava top (left) and welded lapilli tuff (right), Bolhøgdin unit; width of picture ~30 cm (E549748/N6984149). (L) Detail of welded lapilli tuff, Bolhøgdin. (M) Sandstone beds with calcareous, pebbly conglomerate typical of the upper part of the Fjellvollen Formation (E544473/N6982817). (N) Trace fossils in thin-bedded silt- and sandstones of the Fjellvollen Formation. *Curvolithus* isp. (left), *Chondrites* isp. (middle upper), *Protovirgularia* isp. (stretching diagonally from upper right toward lower left). Pen tip for scale (E552060/N6985338). (O) Raudhatten conglomerate. Large angular block of Hølonda Porphyrite (HP), with its characteristic plagioclase-phyric texture, in a light greenish tuffaceous matrix. Other clast types include limestone (L), sandstone (S), and a light-greenish volcanic rock (V) (E547350/N6985200).
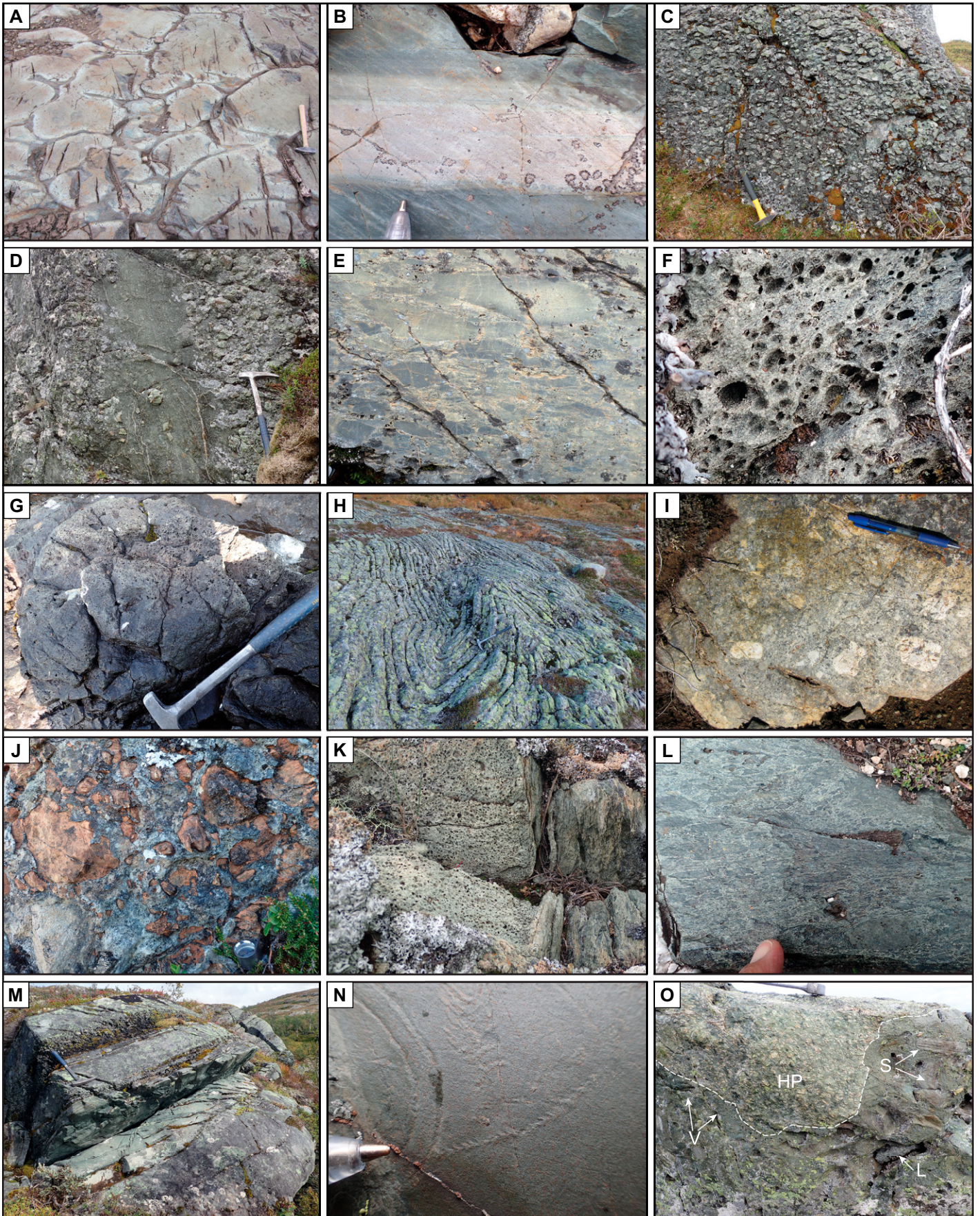
total thickness of up to 30 m and a lateral extent of at least 670 m (Fig. 2C). Lower and middle parts comprise mafic to intermediate, pillowed or massive lava; the underlying limestone is heavily veined by magma and partly exhibits peperitic mingling (Fig. 5J). Vesicularity is mostly low, but highly vesicular (~70%) varieties are seen at the top of flows (Fig. 5K). The upper part of the Bolhøgdin unit includes a mafic welded tuff with lapilli-size clasts (Fig. 5L).

Overlying the Bolhøgdin unit is a ~1.6-km-thick succession of variably calcareous and quartz-rich, gray to greenish-gray turbiditic graywackes, ranging from thick-bedded sandstone with conglomerates (graded beds <6 m thick, channels <2 m deep) to thin (<10 cm) silt-dominated beds (Figs. 3B and 5M) with trace fossils from seafloor-dwelling organisms (Fig. 5N). Complete Bouma sequences are present. Clasts include quartzite, igneous rocks, limestone, jasper, and calcareous sandstone. A general upward coarsening is accompanied by increasing contents of carbonate, and conglomerates in the upper 400–500 m containing up to ~30% limestone clasts.

The turbidites are overlain by the ~200-m-thick Raudhatten unit (Figs. 2C and 3B), which partly fills channels up to 3 m deep in the turbidites. Its lower part is dominated by very coarse, mostly matrix-supported conglomerate with angular to rounded clasts up to 1 m across set in a mafic tuffaceous matrix, separated by thinner (mostly <1 m) mafic tuffaceous beds. The upper part comprises bedded volcaniclastic deposits of similar mafic tuffaceous composition, with internal grading, planar and cross lamination, and trough crossbedding. The Raudhatten conglomerates are characterized by a predominance of mafic volcanic clasts (Fig. 5O), mostly highly plagioclase-phyric and texturally identical to the Hølonda Porphyrites farther northwest (Grenne and Roberts, 1998). Their geochemical composition also conforms to that of the shoshonitic Hølonda Porphyrites (Fig. S3; Table S1). Limestone clasts are abundant, whereas jasper, quartzite, and sandstone are subordinate (Fig. 5O; Walsh, 1986).

Conformably overlying the Raudhatten unit, ~100 m of turbiditic, thin-bedded siltstone and shale are overlain by an up to 150-m-thick unit of pillowed and massive, variably vesicular basaltic lavas, referred to here as the Svartvatna basalts (Figs. 2C and 3B). Intercalated sedimentary breccias are similar to those of the Mostadmarka Formation, comprising clasts and blocks of volcanic material and subordinate jasper.

Føssjøen Formation

The Svartvatna basalts are overlain by a ~1.6-km-thick turbiditic succession dominated by thin-bedded (normally <10 cm but locally up to 1 m) sandstone, siltstone, and shale; intervals of abundant intra-formational conglomerates occur in lower to middle parts. Sedimentary structures include normal grading, loaded bases, rip-up clasts, planar lamination, and current ripples, partly with complete Bouma sequences (Walsh, 1986). Clast composition is similar to that of the Fjellvollen Formation, but sandstones and shales are generally more greenish and feldspathic and contain less carbonate.

GEOCHEMISTRY

Samples for geochemical analysis of volcanic rocks include one from a pillow lava in the Skjøla olistostrome, 16 from the Jonsvatnet Formation, 74 from the Mostadmarka Formation, and 10 from the Fjellvollen Formation (Table S1). Neodymium and Sr isotopes are reported for 14 samples from the Mostadmarka Formation and five from the Fjellvollen Formation (Table S3; see footnote 1). The geochemical composition of the samples was measured by X-ray fluorescence and laser ablation–inductively coupled plasma–mass spectrometry (LA–ICP–MS) at the Geological Survey of Norway, whereas Nd and Sr isotopes were analyzed by TIMS at the British Geological Survey; detailed analytical methods are described in the Supplemental information.

General Outline

The volcanic rocks of the Ilfjellet Group show a conspicuously bimodal chemical composition (Fig. 6). The first group, referred to as MORB-type lavas (80 samples, Table S1), includes more than 99% of the volcanic parts of the Jonsvatnet and Mostadmarka formations and also incorporates the Svartvatna basalts of the Fjellvollen Formation. The second group, referred to as the Th-rich units (31 samples), includes the volumetrically subordinate Gragjelfjellet, Vertjønna, and Slættesberget units of the Mostadmarka Formation and the Jorlisætra and Bolhøgdin units of the Fjellvollen Formation.

The MORB-type lavas are almost exclusively mafic, with only a few intermediate compositions, and have Th contents mostly between 0.1 and 3 ppm (Fig. 6A). By contrast, the Th-rich units are predominantly intermediate to felsic and contain 30–150 ppm Th. The Vertjønna rhyolite is the only sample with more than 69 wt% SiO_2. The contrast between the two main groups of volcanic rocks is confirmed by the discrimination diagram of Pearce (1996) based on immobile high field strength elements (HFSE), where the MORB-type lavas plot mostly as normal basalts and the Th-rich units show similarities to trachyandesite and trachyte to alkali rhyolite (Fig. 6B).

A clear distinction between the two main groups of Ilfjellet volcanic rocks is evident also in a Nb/Yb versus Th/Yb plot (Fig. 6C). Despite a large spread in the trace element ratios, nearly all basalts fall within the MORB-ocean island basalt (OIB) Array of Pearce and Peate (1995), clearly different from arc-related magmas. Five samples from the Mostadmarka Formation have slightly elevated Th/Yb ratios and plot just outside of the MORB-OIB Array. By contrast, the Th-rich units plot far above the MORB-OIB Array and also far outside the fields for normal arc magmas (Fig. 6C).

A Note on Nomenclature

The terminology of MORB-type magma compositions is inconsistent in modern literature. A common reference is that of Sun and McDonough (1989), who distinguished between normal (N)-MORB and enriched (E)-MORB. But also depleted (D)-MORB and transitional (T)-MORB have been used in the literature based on varying definitions. Gale et al. (2013) suggest a revised nomenclature for MORB based on a comprehensive study of all available data on modern MORB, excluding back-arc settings. In their definition, N-MORB is the most likely basalt composition encountered along ridges >500 km from hot spots, while D-MORB and E-MORB are defined by primitive-mantle-normalized La/Sm ratios <0.8 and >1.5, respectively. In this contribution we follow the definitions of D- and E-MORB of Gale et al. (2013). The term N-MORB, however, is avoided here since the previous definition of Sun and McDonough (1989) overlaps with the recent definition of D-MORB (Fig. 6C). Instead we use the term T-MORB for our samples falling between D- and E-MORB compositions.

Thorium may serve as a proxy for mobile potassium (Hastie et al., 2007), and the Th-rich rocks of the Ilfjellet Group share many geochemical similarities with ultrapotassic rocks (Foley et al., 1987; Mitchell and Bergman, 1991). However, the correct nomenclature for the primary, igneous protoliths of our Th-rich rocks is difficult to determine due to the probability of severe modifications of the alkali elements during alteration and metamorphism. This is particularly problematic with originally ultrapotassic rocks where leucite may be the major phase, since leucite rapidly degrades to analcime through an exchange of K by Na, leading potentially to extensive loss of K (Giampaolo et al., 1997; Prelević et al., 2004). Moreover, the many different classification schemes for highly potassic rocks (e.g., Conticelli et al., 2010) are based largely on primary mineralogy and hence cannot be directly applied to our rocks.
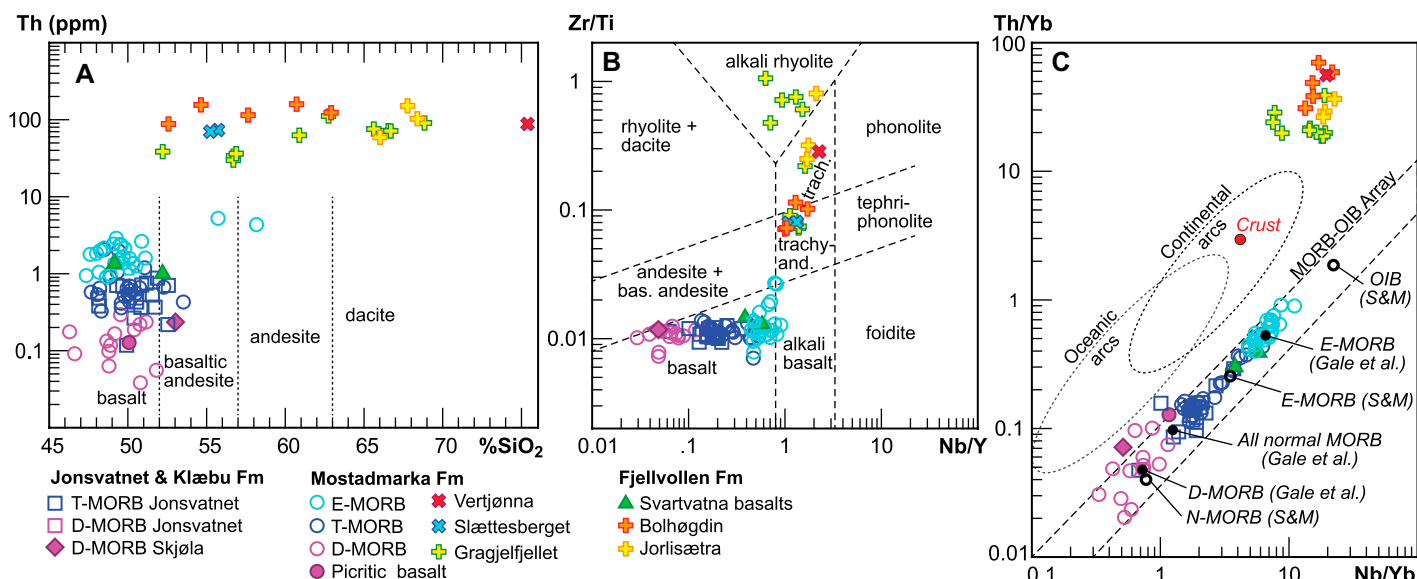
Figure 6. General geochemical characteristics of the Ilfjellet Group volcanic rocks. For sample locations, see Figure 2. (A) SiO$_2$ versus Th showing the highly enriched nature of the predominantly intermediate and felsic rocks of the Gragjelfjellet, Slættesberget, Vertjønna, Jorlisætra, and Bolhøgdin units, in contrast to the basalt-dominated mid-ocean ridge basalt (MORB)-type rocks. See text for subdivision of MORB into depleted (D)-, transitional (T)-, and enriched (E)-MORB. Data are normalized to volatile-free compositions for SiO$_2$ values to conform with standard TAS classification. (B) Geochemical classification of the Ilfjellet volcanic rocks based on the stable elements Zr, Ti, Nb, and Y (Pearce, 1996), showing the separation into one group of essentially basaltic rocks and another group of trachytic affinity. (C) Th/Yb versus Nb/Yb plot (Pearce, 2014) with fields for typical volcanic arc and MORB–ocean island basalt (OIB) rocks. Data for average normal (N)-MORB, E-MORB, and OIB from Sun and McDonough (1989) (S&M). Also shown are average D-MORB and E-MORB, and "all normal MORB" (global average of all MORB far from mantle plumes and excluding back-arc basin basalts) as defined by Gale et al. (2013). Note that average D-MORB of Gale et al. (2013) is close to average N-MORB of Sun and McDonough (1989). Average continental crust from Rudnick and Gao (2003). Fm—Formation; bas.—basaltic.

The MORB-type Lavas

Of our 80 MORB-type samples, 19 (24%) are classified as D-MORB, 35 (44%) as T-MORB, and 26 (32%) as E-MORB. Their spatial distribution (Figs. 2 and 3) demonstrates that D-MORB occurs mainly at low stratigraphic levels of the Mostadmarka Formation, while E-MORB predominates in the upper parts of the Mostadmarka Formation and the Svartvatna basalts of the Fjellvollen Formation. The Jonsvatnet Formation and middle parts of the Mostadmarka Formation are dominated by T-MORB.

The Mg# (mostly ∼69–36; Fig. S4A; Table S1) are significantly lower than in primary mantle melts (Mg# 72; Niu and O'Hara, 2008) and also mostly lower (more evolved) than average MORB (Mg# ∼60; White and Klein, 2014). There are large variations within each MORB group, particularly in T-MORBs of the Jonsvatnet Formation that have Mg# of 66–37 and in E-MORBs of the Mostadmarka Formation that have Mg# generally at 60–38 and as low as ∼30–15 in two samples of basaltic andesite and andesite (Fig. S4A). The contents of Fe$_2$O$_3$$^{(total)}$ and TiO$_2$ generally increase with decreasing Mg# (Table S1), and many T- and E-MORB

samples have high Fe (up to 14.0 wt%) and TiO$_2$ (up to 3.21 wt%) contents comparable to ferrobasalt (Natland, 1980; Perfit, 2001). Rare picritic basalt associated with D-MORB lavas has 22.1 wt% MgO, 2000 ppm Cr, and 739 ppm Ni at 46.8 wt% SiO$_2$ (Table S1).

The MORB-type basalts have trace element patterns that are consistent with the large spread along the MORB-OIB Array field (Fig. 6C). Chondrite-normalized rare earth element (REE) patterns (Fig. 7A) grade from a few samples with strong depletion in light (L)-REE and convex-upward curves, to many samples with markedly LREE-enriched patterns; La/Lu$_N$ ratios (chondrite-normalized; Sun and McDonough, 1989) vary from 0.33 to 2.54 (Table S1). Europium anomalies are insignificant or moderately positive; the positive anomalies are attributable to accumulation of abundant plagioclase phenocrysts.

Mantle-normalized multielement patterns (Fig. 7B) are also broadly comparable to modern MORB. All groups have generally smooth patterns that range from strongly depleted to consistently enriched in the most incompatible HFSE. None of our samples show geochemical patterns characteristic of arc-related magmas, such

as large negative Nb-Ta anomalies (e.g., Pearce, 2014). The five D- and T-MORB samples that plot just outside of the MORB-OIB Array field in Figure 6C have very small negative Nb-Ta anomalies and deviate only little from modern MORBs (Fig. 7B).

Compared to typical modern MORBs, our MORB-type samples have higher ratios of middle (M)-REE to heavy (H)-REE, e.g., Sm/Yb$_N$ ratios of 1.25–1.76 for the D-MORBs and 1.38–2.64 for the T-MORBs (Table S1). This is reflected also in the strikingly upward-convex REE patterns (Fig. 7A). Similarly, our E-MORBs have elevated MREE/HREE ratios (Sm/Yb$_N$ = 1.98–3.05; Table S1) and relative enrichments of Zr, Hf, and Ti compared to typical modern E-MORB (Figs. 7A and 7B). The discordance is seen also in the TiO$_2$/Yb versus Nb/Yb diagram (Fig. S4B), where the E-MORBs have geochemical signatures more akin to tholeiitic OIB (Pearce, 2014).

Chromium varies mostly from ∼40 to 500 ppm and Ni from ∼30 to 230 ppm, excluding the picritic basalt and the two intermediate samples. The moderately incompatible HFSE generally correlate well with TiO$_2$ and P$_2$O$_5$ over large ranges (e.g., 42–241 ppm
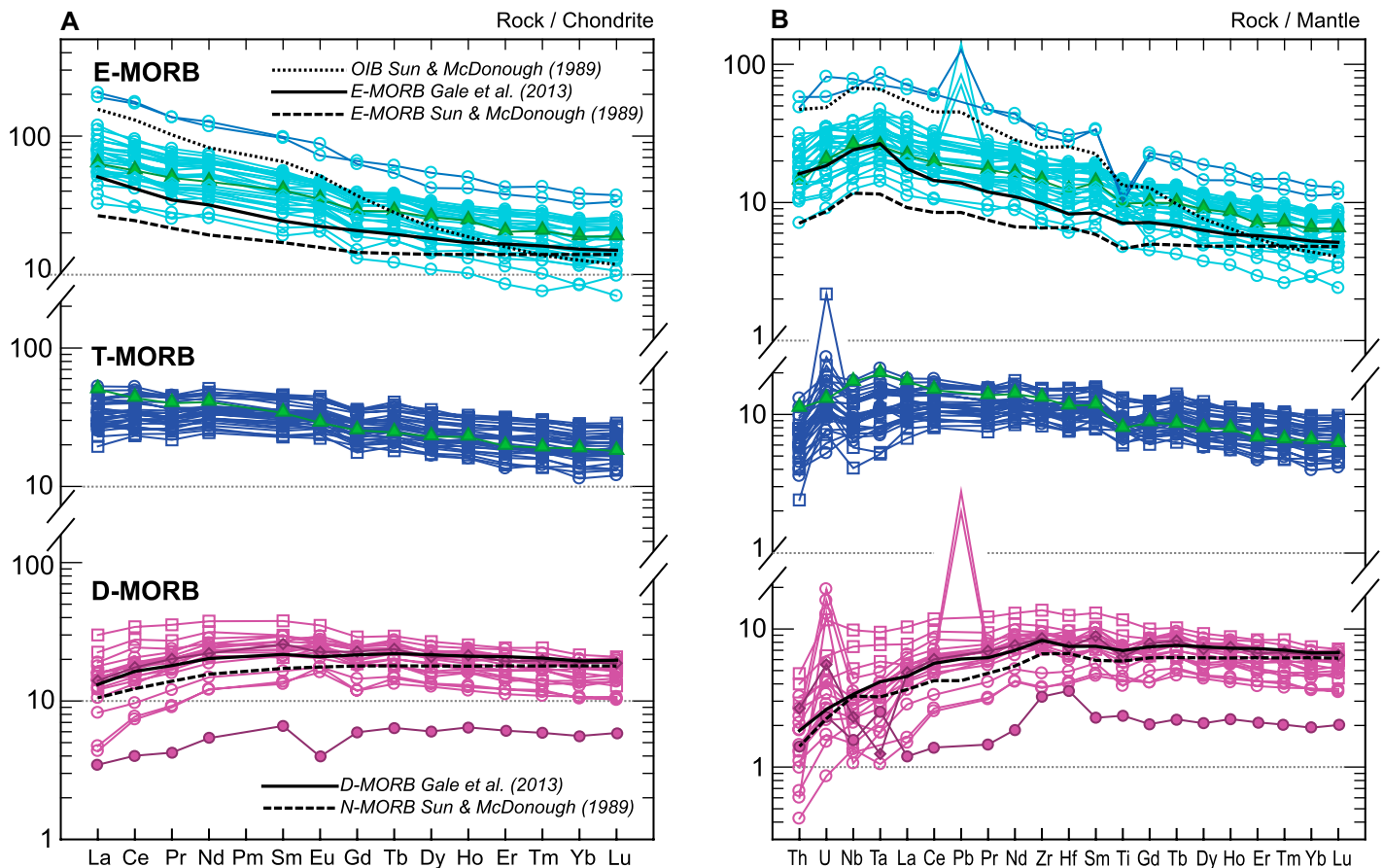
Figure 7. Trace element patterns for the mid-ocean ridge basalt (MORB)-type lavas of the Ilfjellet Group. For sample locations, see Figure 2. (A) Chondrite-normalized rare earth element patterns. (B) Primitive-mantle-normalized patterns. Chondrite and primitive mantle values from Sun and McDonough (1989). Note that there is a gradual variation from depleted-mid-ocean ridge basalt (D-MORB), through transitional (T)-MORB, to enriched (E)-MORB compositions, and that the separation is only for descriptive purposes. The apparent positive Pb anomaly in six samples is thought to be an artifact of analytical uncertainty at concentrations at or near the quantification limit (the quantification limit of 5 ppm Pb is nearly two orders of magnitude above the normalizing value of 0.071 ppm). Average D-, N-, E-MORB and ocean island basalt (OIB) compositions of Gale et al. (2013) and Sun and McDonough (1989) are shown for comparison. Symbols as in Figure 6.

Zr). Concentrations of the most incompatible HFSE vary by up to two orders of magnitude, as reflected in the mantle-normalized diagram (Fig. 7B); for example, Th ranges from 0.04 to 2.69 ppm.

The Th-rich Units

The Gragjelfjellet, Slættesberget, Jorlisætra, and Bolhøgdin units are generally significantly enriched in highly incompatible large-ion litho-phile elements (LILE), such as K_2O and Ba, compared to the MORB-type lavas (Fig. S5; Table S1). The interior of a thick, massive lava flow of intermediate SiO_2 in the Gragjelfjellet unit has nearly 10 wt% K_2O (sample TGR19_30) and the two samples of pillow lava at Slættesberget have consistently high K_2O (5.61–6.60 wt%) and Ba (1100–1130 ppm). Moreover, the large spread of

K_2O (and Ba, Rb, Cs) and K_2O/La ratios, which is particularly evident in the Bolhøgdin unit (Table S1; Fig. S5), indicates extensive loss of the mobile LILE and that the higher K_2O values are closer to primary compositions. This is in accordance with their likely ultrapotassic character as estimated from high Th contents.

MgO shows an erratic negative correlation with SiO_2, with more than 9 wt% MgO in one mafic sample (Fig. 8A). The Al_2O_3 contents of ~14–18 wt% (Fig. 8B) are significantly higher than in lamproitic rocks (Foley et al., 1987), which otherwise share many trace element characteristics of the Ilfjellet Th-rich units. TiO_2 (0.14–1.57 wt%) and P_2O_5 (0.07–1.40 wt%) are inversely correlated with SiO_2 (Figs. 8C and 8D); P_2O_5 values in more mafic varieties are far above those of the MORB-type rocks (Fig. 8D). Concentrations of moderately incompatible HFSE

are generally high (e.g., 451–1760 ppm Zr; Fig. 8E). The highly incompatible trace elements are extremely enriched, with 28.4–147.0 ppm Th (Fig. 6A) and 9.0–36.3 ppm U. Concentrations of Be (1.8–18.9 ppm) and Sn (6–20 ppm) are also much higher than those of the MORB-type lavas (Fig. 8F; Table S1). Noticeably, the highly incompatible trace elements show little or no correlation with SiO_2 (Fig. 8).

Ni and Cr contents are highly variable at similar SiO_2 levels, particularly in the Bolhøgdin unit (Figs. 8G and 8H). Some of these intermediate rocks have Ni and Cr concentrations far above those of other comparable rocks from the Th-rich units, and also far higher than the values of the basaltic MORB-type volcanic rocks.

REE and trace element patterns (Fig. 9) contrast strongly with those of the Ilfjellet MORB-type lavas. Chondrite-normalized LREE/HREE
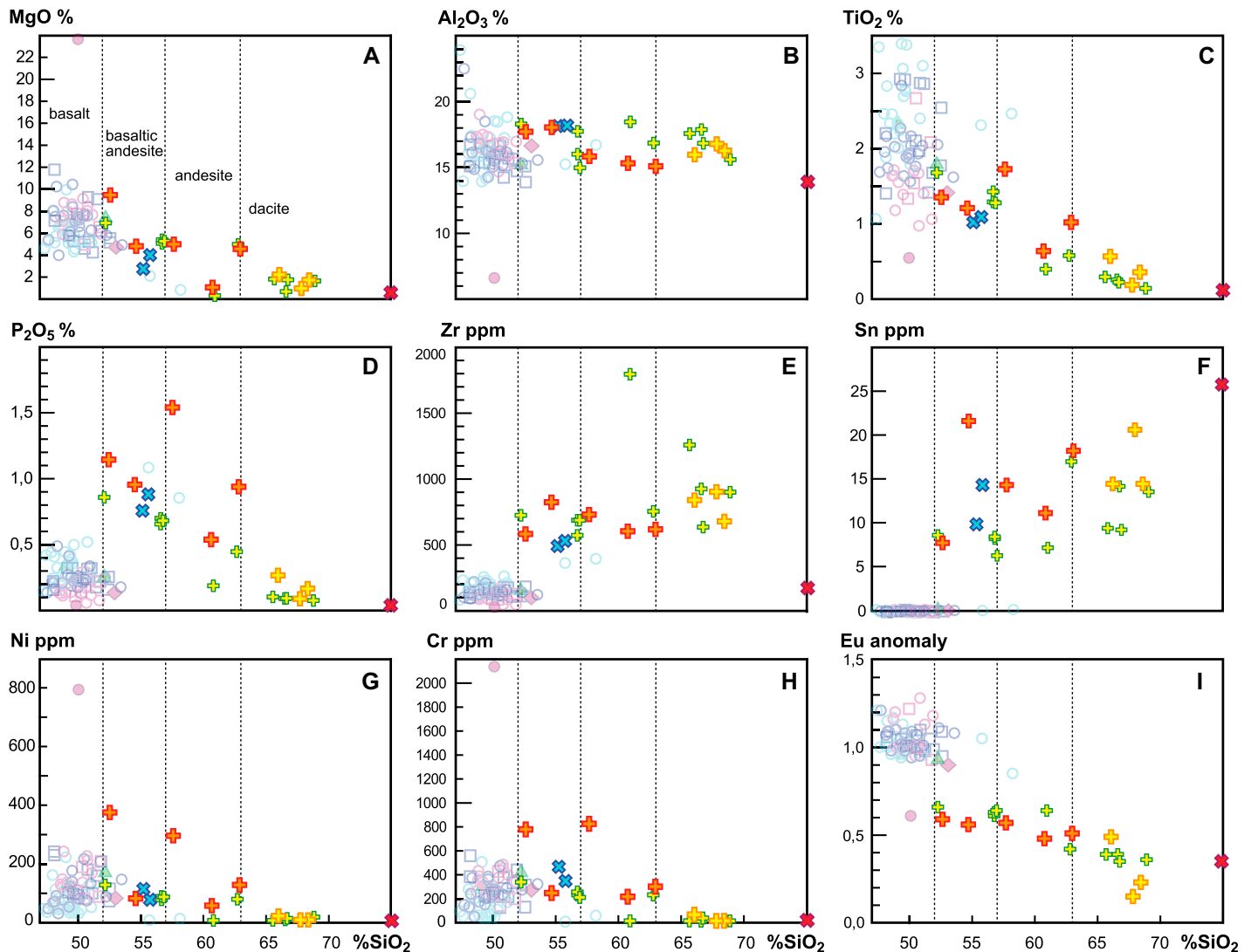
Figure 8. Binary geochemical plots for the Th-rich volcanic units of the Ilfjellet Group. For sample locations, see Figure 2. Symbols as in Figure 6; the mid-ocean ridge basalt-type lavas are shown in light tones for comparison. All data are normalized to volatile-free compositions for SiO$_2$ values to conform with standard TAS classification.

ratios are very high, while the HREE patterns are relatively flat. Europium anomalies are ∼0.7 in the least evolved rocks and are consistently more negative toward more evolved compositions (Figs. 8I and 9A). The rocks display marked negative anomalies for Nb-Ta and large positive Pb anomalies (Fig. 9B). Within the different Th-rich units, trace element patterns are nearly parallel over relatively large SiO$_2$ ranges.

The Bolhøgdin and Slættesberget units show a peculiar, flat or upward-convex, pattern for the LREE, different from the steep LREE pattern of the Gragjelfjellet and Jorlisætra units (Fig. 9A), and they differ also by relative enrichments in W (3.12–12.6 ppm). The Vertjønna rhyolite is unique, having higher SiO$_2$ (∼75 wt%), a shallower REE pattern and a smaller negative Eu

anomaly despite its more evolved character in terms of SiO$_2$ (Figs. 8B and 9A). The rhyolite also displays a stronger enrichment of Th and U relative to the less incompatible HFSE (Fig. 9B), a very large positive Pb anomaly and elevated concentrations of Be and Sn (Table S1).

Similarly enriched volcanic rocks have recently been documented by Dalslåen et al. (2020a, 2020b) in units of overlapping age (ca. 475–470 Ma) farther south (the Kinna volcanic succession, the Storgruvpiken rhyolite, and rhyolites within the Trollhøtta unit; Fig. 2A). Notably, the Storgruvpiken rhyolite shows striking similarities to the Vertjønna rhyolite, including very high Be (up to 66.5 ppm) and Sn (up to 31.6 ppm).

Rb-Sr and Sm-Nd Isotopes

The Rb-Sr and Sm-Nd isotope data of the volcanic rocks fall in two main groups, consistent with the geochemical subdivision above. The MORB-type lavas yield initial ^{87}Sr/^{86}Sr (Sr$_i$) between 0.7040 and 0.7088, and εNd$_t$ between 4.8 and 9.4, whereas the Th-rich units have Sr$_i$ between 0.7089 and 0.7175 and εNd$_t$ between −8.0 and −6.6 (Fig. 10A; Table S3). Depleted-mantle model ages for the Th-rich units range from 1.7 to 1.3 Ga (Fig. 10B), indicative of significant input of Proterozoic crustal material.

The Nd isotopic compositions of the MORB-type lavas are strongly correlated with elemental ratios, such as La/Sm, that reflect mantle-source depletion and distinguish D- and E-type MORB
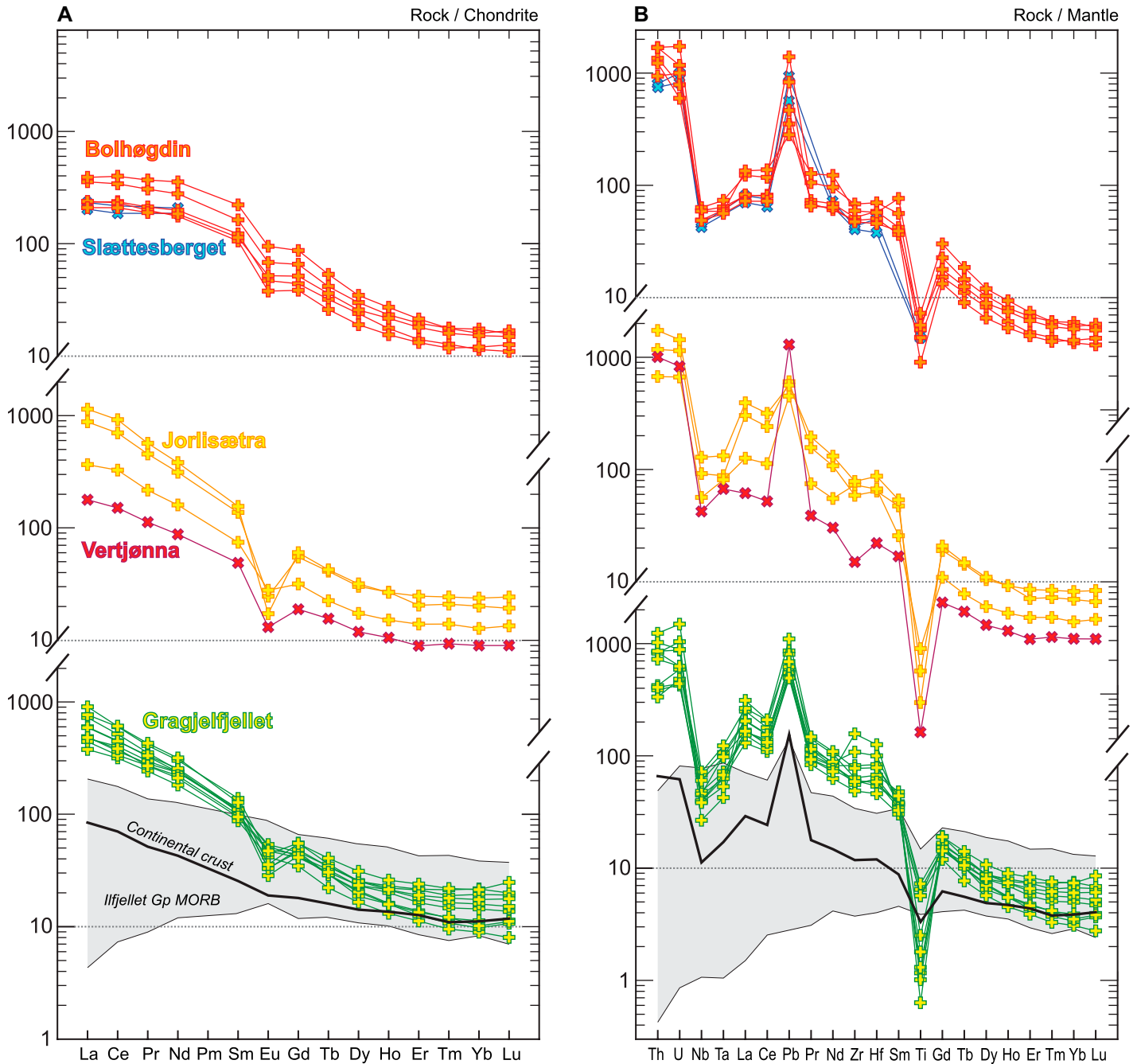
Figure 9. Trace element patterns for the Th-rich volcanic units of the Ilfjellet Group (Gp). For sample locations, see Figure 2. (A) Chondrite-normalized rare earth element patterns. (B) Primitive-mantle-normalized patterns. Chondrite and primitive-mantle values from Sun and McDonough (1989). The composition of the Ilfjellet basalts, as well as the average composition of continental crust (Rudnick and Gao, 2003) are shown in the lowermost graph for comparison. Symbols as in Figure 6. MORB—mid-ocean ridge basalt.

(Fig. 10C). The isotopically most depleted samples classify as D-MORB and the more evolved samples as E-MORB. The negative correlation of εNd_t with La/Sm (Fig. 10D) and the lack of correlation with Th/Nb (Fig. 10D), the latter serving as an indicator of crustal contamination, indicate that the compositional variations observed in the MORB-type lavas are mainly related to heterogeneous mantle sources rather than variable assimilation of crust. This observation is consistent with the general lack of negative Nb-Ta anomalies in the mantle-normalized plots (Fig. 7B). The Th-rich lavas have tightly clustered εNd_t values, but a relatively large spread in Sr_i that is largely uncorrelated with chemical composition.

GEOCHRONOLOGY

The Gragjelfjellet, Jorlisætra, and Bolhøgdin Th-rich units were sampled for U-Pb TIMS dating of zircon and four sandstone samples from the Klæbu and Fjellvollen formations were selected for detrital zircon U-Pb LA–ICP–MS dating. U-Pb TIMS analyses were performed at
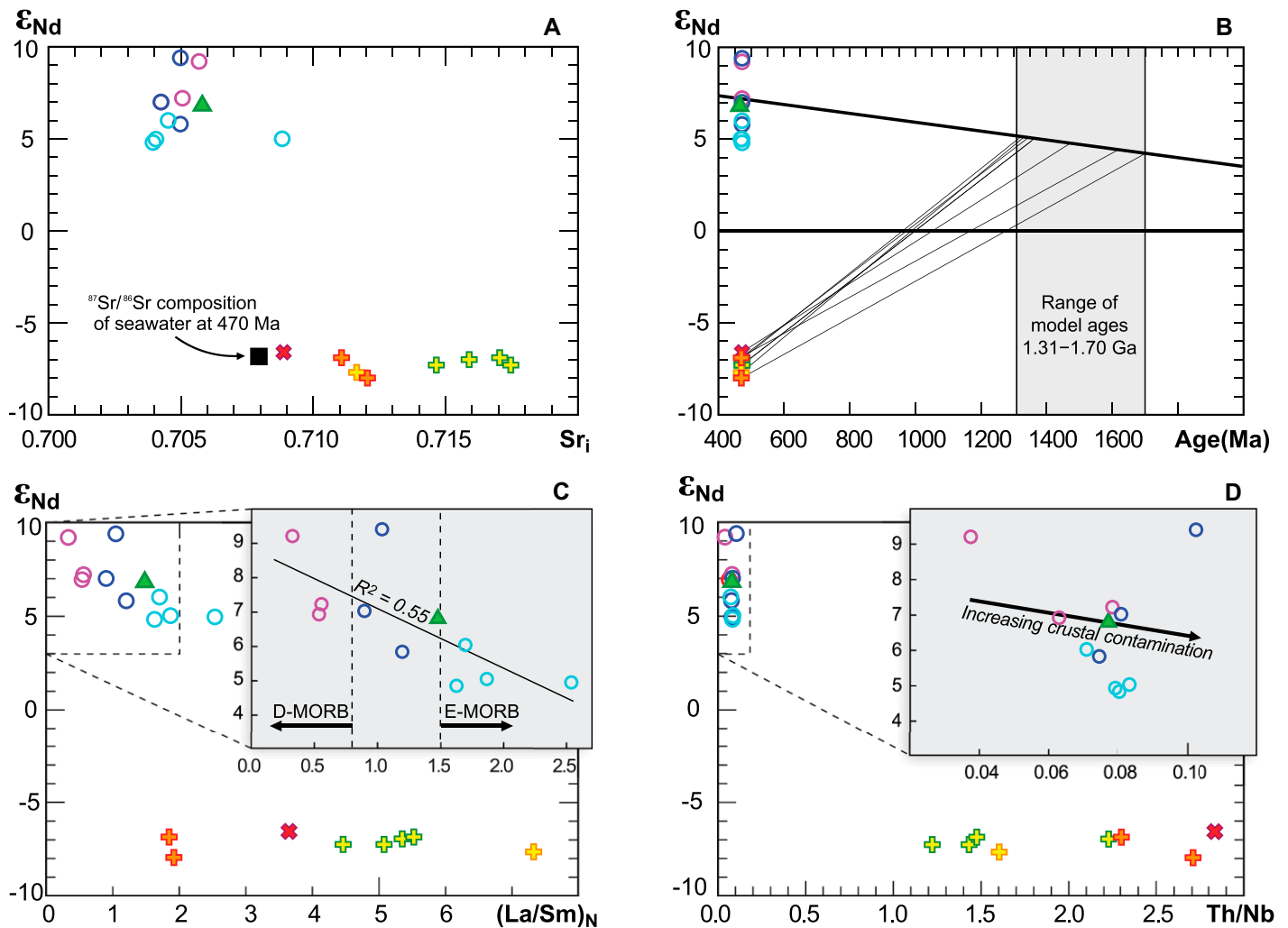
Figure 10. Rb-Sr and Sm-Nd isotope data for the Ilfjellet volcanic rocks. For sample locations, see Figure 2. (A) Initial Sr (Sr$_i$) versus εNd for mid-ocean ridge basalt (MORB)-type lavas and Th-rich units, calculated for the time of crystallization determined by U-Pb zircon geochronology. The black square shows the $^{87}Sr/^{86}Sr$ composition of seawater at 470 Ma (after Veizer et al., 1999). Concentrations of Nd in seawater are very low (on the order of 10^{-11} mol/kg) compared to Sr (10^{-4} mol/kg) and therefore unlikely to affect the composition of rocks during hydrothermal alteration. Alteration by seawater is therefore expected to produce horizontal trends in Sr$_i$ vs εNd plots, as observed for the data presented here. (B) Age versus εNd indicating depleted-mantle model ages for the Th-rich units. (C) εNd versus La/Sm$_N$ (chondrite-normalized) showing that—unlike the Th-rich units—εNd in the MORB-type lavas is correlated with these ratios, consistent with a transition from depleted (D)-MORB to enriched (E)-MORB. (D) Plot showing that εNd in neither unit is correlated with Th/Nb, the latter a sensitive indicator of crustal contamination. Symbols as in Figure 6.

the Department of Geosciences at the University of Oslo, Norway, following the procedures described in Augland et al. (2010) and Ballo et al. (2019), whereas the U-Pb LA–ICP–MS analyses were performed at the Geological Survey of Norway. A detailed description of the analytical methods can be found in the Supplemental information.

U-Pb TIMS Dating of Volcanic Rocks

Sample V1 (TGR16_305) is from a trachytic lava flow in the Gragjelfjellet unit south of Ilfjellet (Figs. 2C and 3B). The zircon population from this sample consists of euhedral and equant to short-prismatic crystals (Fig. S6). Of five analyses, four overlap on concordia and one is younger than the main cluster. The four overlapping fractions give a mean $^{206}Pb/^{238}U$ age of 473 ± 1 Ma (Fig. 11A; Table S2).

Sample V2 (TGR14_223) is a tuff of trachytic affinity from the Jorlisætra unit at the base of the Fjellvollen Formation (Figs. 2C and 3B). The extracted zircon grains are rather heterogeneous in shape and color (Fig. S6). There are equant, euhedral, mostly brown and translucent crystals. Others occur mainly as clear transparent fragments, locally with euhedral faces. Clear zircon

is seen overgrowing brown zircon and vice-versa. Four fractions were analyzed: clear zircons were chemically abraded and two brownish zircons were air abraded. The two brown grains were very rich in U, up to >1%. One analysis is very imprecise and the other discordant. The two clear grains have much lower U contents and yield concordant data, but also show some dispersion. The overall pattern combined with the appearance and U contents of the grains indicate that younger apparent ages are due to partial Pb loss. The oldest $^{206}Pb/^{238}U$ age of 473 ± 1 Ma of a large clear tip is considered the most reliable estimate of the age of crystallization (Fig. 11B; Table S2).
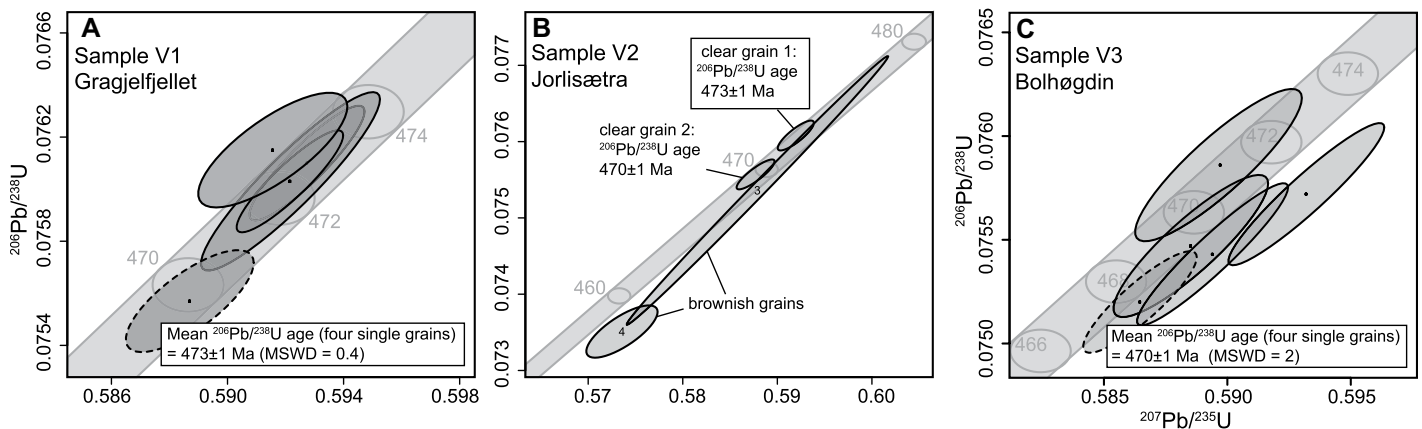
Figure 11. Concordia plots for the zircon U-Pb thermal ionization mass spectrometry data. For sample locations, see Figure 2. Data-point ellipses are 2σ; plots are made with Isoplot (Ludwig, 2003). MSWD—mean square weighted deviation.

Sample V3 (TGR15_408) is a lava of trachytic affinity from the Bolhøgdin unit of the Fjellvollen Formation (Figs. 2C and 3B). Zircon occurs as short-prismatic, euhedral crystals, commonly fragmented (Fig. S6). The grains range from colorless to brown-red, the latter reflecting high U contents (880–2700 ppm U in the measured grains). Five zircon analyses are clustered around the concordia curve. Four of them have overlapping $^{206}Pb/^{238}U$ ages with a mean of 470 ± 1 Ma. The fifth analysis is slightly younger, likely due to some Pb loss from U-rich domains (Fig. 11C; Table S2).

LA–ICP–MS Dating of Detrital Zircon

Sample S1 (TGR_33) is a sandstone from the Klæbu Formation (Figs. 2B and 3A; Table S4). Of 99 analyses performed on 99 grains, 46 are <10% discordant and fall into three age groups: (1) Archean (ca. 3200–2700 Ma, 6 grains, 13%), (2) Paleo- to Mesoproterozoic (2000–1000 Ma, 13 grains, 28%), and (3) Cambro-Ordovician (ca. 500–440 Ma, 27 grains, 59%) (Fig. 12A). Of 27 Cambro-Ordovician analyses, 12 are <5% discordant. The different methods to estimate the maximum depositional age (MDA) give 448 ± 5 Ma (YSG—youngest single grain, 1% discordant), 463 ± 6 Ma (YGC—youngest grain cluster with n^3 and 2σ overlap), and ca. 475–480 Ma (YPP—youngest graphical peak in the Kernel density estimate curve). See Coutts et al. (2019) for details on methods for estimating MDA.

Sample S2 (TGR14_020) is a sandstone from the Jonsvatnet Formation at Hyttfossen (Figs. 2B and 3A; Table S4). Of 111 analyses performed on 111 grains, 81 are <10% discordant and fall into three age groups: (1) Archean (ca. 3000–2600 Ma, 9 grains, 11%), (2) Paleo- to Mesoproterozoic (1900–1000 Ma, 16 grains, 20%), and (3) Cambro-Ordovician (ca. 600–450 Ma,

56 grains, 69%) (Fig. 12B). Of 56 Cambro-Ordovician analyses, 38 are <5% discordant. The different methods to estimate the MDA give 450 ± 5 Ma (YSG, +3% discordant), 457 ± 6 Ma (YGC 2σ) and ca. 485 Ma (YPP).

Sample S3 (TGR15_583) is a sandstone from the lower part of the Fjellvollen Formation (Figs. 2C and 3B; Table S4). Of 100 analyses performed on 100 grains, 92 are <10% discordant and fall into three age groups: (1) Archean (ca. 3100–2600 Ma, 6 grains, 6%), (2) Paleo- to Mesoproterozoic (2100–900 Ma, 55 grains, 60%), and (3) Cambro-Ordovician (ca. 500–450 Ma, 31 grains, 34%) (Fig. 12C). Of 31 Cambro-Ordovician analyses, 29 are <5% discordant. The different methods to estimate the MDA give 434 ± 4 Ma (YSG, 4.7% discordant), 465 ± 5 Ma (YGC 2σ), and ca. 480–485 Ma (YPP).

Sample S4 (TGR15_10) is a sandstone from the upper part of the Fjellvollen Formation (Figs. 2C and 3B; Table S4). Of 100 analyses performed on 100 grains, 80 are <10% discordant and fall in three age groups: (1) Archean (ca. 2900–2400 Ma, 17 grains, 21%), (2) Paleo- to Mesoproterozoic (ca. 1900–1000 Ma, 28 grains, 35%), and (3) Cambro-Ordovician (ca. 500–450 Ma, 35 grains, 44%) (Fig. 12D). Of 35 Cambro-Ordovician analyses, 18 are <5% discordant. The different methods to estimate the MDA give 456 ± 4 Ma (YSG, 3% discordant), 465 ± 5 Ma (YGC 2σ), and ca. 475–480 Ma (YPP).

DISCUSSION

The Age of the Mostadmarka Formation and its Implications for Stratigraphic Terminology

The U-Pb TIMS zircon age of 473 ± 1 Ma of the Gragjelfjellet volcanic unit in the

Mostadmarka Formation is ∼10 m.y. younger than the LVB ophiolite. These units therefore belong to two fundamentally different volcanic successions. In order to avoid future terminological confusion, we propose that the term Støren Group, which has been used both for the LVB ophiolite and the Mostadmarka Formation, be abandoned.

Deposition within a Marginal Volcano-Sedimentary Basin

At Vassfjellet, early sedimentation on top of the tilted and deeply eroded ophiolite is reflected by the Skjøla olistostrome of the Klæbu Formation. This thick olistostrome indicates an unstable rift setting with intermittent, local D-MORB volcanism and active tectonism leading to large-scale mass flows on steep slopes, dissected by canyons. The overlying turbidites of the Klæbu Formation are interpreted to reflect increasing water depths or a larger distance to the adjacent landmass. In the lower part of the formation, thick and coarse-grained turbidites deposited on proximal submarine fans alternate with finer grained turbidites deposited in levee settings, possibly reflecting along-strike variations in deposition.

The subsequent submarine basalts of the Jonsvatnet Formation, characterized by T-MORBs, oxidic iron formation and minor jasper, compare geochemically and lithologically well with the middle parts of the much thicker Mostadmarka Formation (Fig. 3). This suggests that the Jonsvatnet and Mostadmarka basalts formed in different parts of the basin, the latter inferably closer to a central rift where volcanism started earlier and continued longer.

The basalts in the lowermost parts of the Mostadmarka Formation are associated with sulfide iron formation that is locally rich in
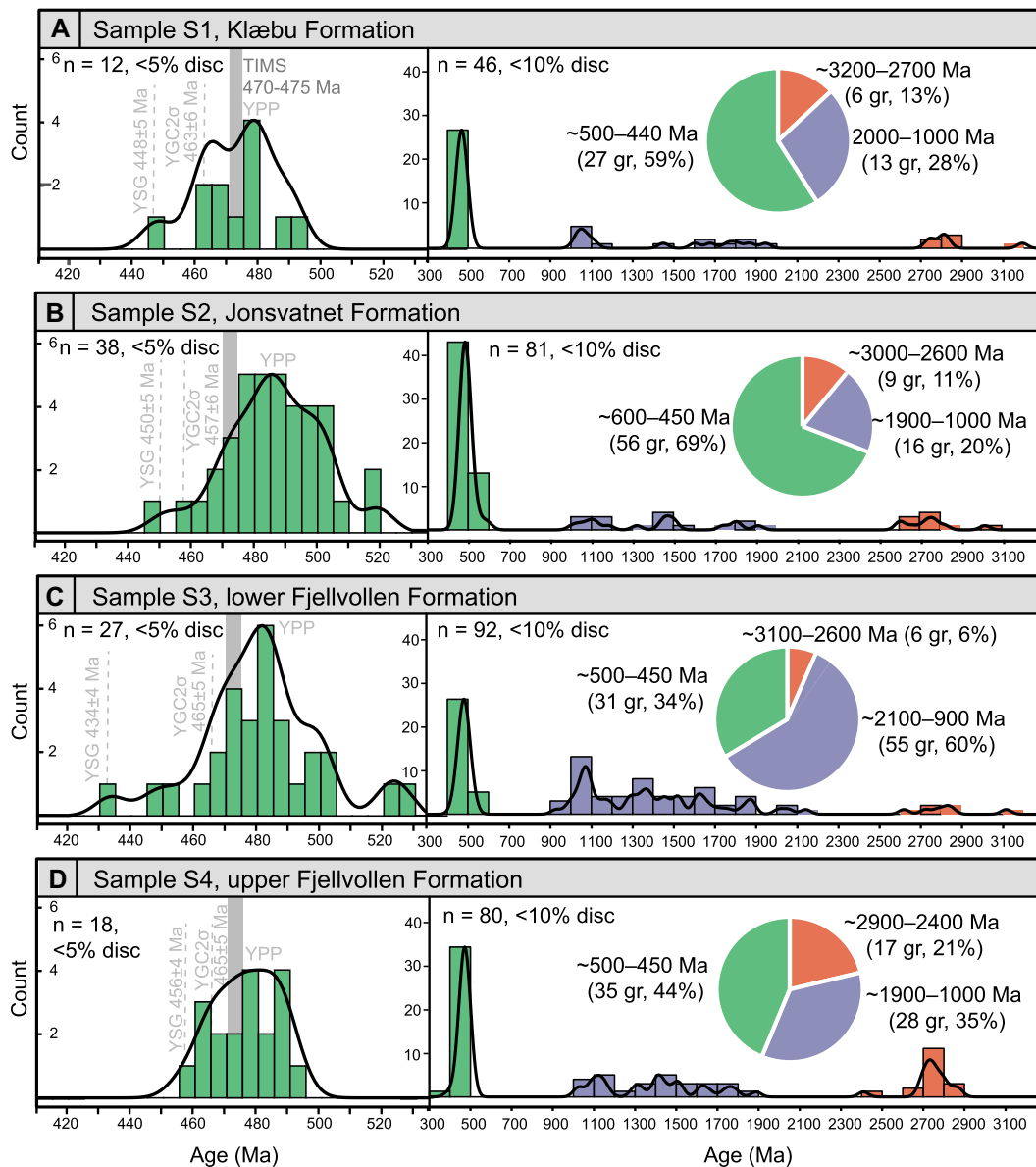
Figure 12. Histograms, kernel density estimates, and cake plots for four detrital zircon samples from the Ilfjellet Group. For sample locations, see Figure 2. For the left-hand plots, bin- and bandwidths are 5; for the right-hand plots, binwidth is 100 and bandwidth is 25. TIMS—thermal ionization mass spectrometry; n—number of included analyses; YPP—youngest graphical peak on the Kernel density estimates.

graphite, implying a restricted, anoxic and partly euxinic setting (Grenne and Slack, 2019). A limited terrigenous input is demonstrated by the virtual absence of siliciclastic sediments, and the low vesicularity (<1%) of the MORB-type lavas points to great water depths, probably >2 km based on comparison with tholeiitic basalts with inferably similar volatile contents in modern settings (de Wit et al., 2020).

The Gragjelfjellet Th-rich unit in the middle part of the Mostadmarka Formation represents a striking anomaly in the volcanic development of the otherwise MORB-dominated succession. The absence of MORB-type lavas or sedimentary deposits between separate internal eruptions implies that the entire Gragjelfjellet sequence formed within a short time interval, and it was immediately succeeded by more

MORB lavas. The much higher vesicularity in parts of the Gragjelfjellet unit as compared to the MORB-type lavas below and above, likely reflects the elevated volatile contents characteristic of evolved magmas with subduction signature versus tholeiitic MORB-type magmas (Wallace, 2005; de Wit et al., 2020).

Submarine volatile-driven explosivity, as evidenced in the Gragjelfjellet unit, is in general greatly limited by the confining water pressure (e.g., Allen et al., 2010). Pyroclastic eruptions have been recorded in modern settings, such as the Kermadec arc (south Pacific Ocean), at depths of 900–1200 m (Carey et al., 2018), but these are pumiceous and not directly comparable to the Gragjelfjellet deposits. Significantly reduced exsolution of volatiles from magmas with increasing water depth leads not only to

lower vesicularity, but also to greatly reduced viscosity; hence very deep water (>1.45 km) eruptions are likely characterized by less vesicular pyroclasts and effusive, rather than explosive, deposits (Busby, 2005; Kessel and Busby, 2003). The volcanic deposits at Gragjelfjellet are consistent with such a deep water setting, in which pressure-related retention of magmatic volatiles facilitated formation of highly fluid and laterally extensive felsic lava together with welded lapilli. The latter were inferably deposited from fire-fountains where an insulating steam cupola protected pyroclasts from rapid cooling (Busby, 2005).

The appearance of thick, basalt-dominated sedimentary breccias in the upper part of the Mostadmarka Formation points to a steep seafloor relief. The angular shape and large size

of clasts, together with abrupt lateral thickness variations, indicate local derivation. The presence of MORB clasts with a vesicularity of up to 5% suggests that some of the basaltic detritus had erupted at shallower water depths (~1 km or less; de Wit et al., 2020). This is tentatively interpreted as reflecting the emergence of steep-sided volcanic seamounts; at the same time deeper parts of the basin received terrigeneous sediments as represented by the thin-bedded turbiditic sand- and siltstones between some lava flows at this stratigraphic level.

The transition into the turbidite-dominated Fjellvollen Formation marks a tectonically unstable depositional environment, witnessed by chaotic sedimentary breccias and soft-sediment deformation. The Th-rich units at Slættesberget (lava) and at Vertjønna and Jorlisætra (pyroclastic) are closely associated with this phase. The Jorlisætra deposits, with their generally angular clasts and little epiclastic material, can be interpreted as subaqueous pyroclastic mass flows from a local source. The slightly younger Bolhøgdin volcanism, represented both by lavas and welded lapilli, probably also formed in a relatively deep-marine setting given the association with under- and overlying turbidites and a similar volcanic facies as the Gragjelfjellet unit. The coexistence of the Bolhøgdin unit with locally underlying ribbon chert and limestone denotes a period of limited or no detrital sedimentation in the volcanically active area, possibly related to magmatic inflation of the seafloor prior to eruption (e.g., Di Vito et al., 2016; Acocella, 2019) that temporarily inhibited deposition from turbidity currents.

The thin-bedded siltstones and shales of the Fjellvollen turbidites reflect far-traveled mass flows from an adjacent landmass, with trace fossil assemblages suggesting bathyal to abyssal water depths (Seilacher, 1967; Smelror et al., 2020). The upper part of the Fjellvollen Formation, characterized by increasing proportions of proximal turbidites and channel deposits with abundant conglomerates, indicates a change in depositional setting to mid-fan and inner fan. This may have resulted from suprafan lobe switching and lobe progradation and shallowing due to filling of the basin (e.g., Covault, 2011).

Toward the Raudhatten unit, a highly calcareous matrix and abundant limestone clasts indicate derivation from a carbonate platform, and the appearance of Hølonda Porphyrite clasts in the Raudhatten conglomerates establishes a clear link to the Hølonda terrane as a source for the limestone and volcanic detritus (Grenne and Roberts, 1998). Bruton and Bockelie (1980) interpreted the setting of the Hølonda Porphyrites as limestone-surrounded islands characterized by lava flows as well as explosive volcanic

deposits; the Raudhatten conglomerates possibly represent mass flows derived from these volcanic islands. The Svartvatna basalts reflect a new, brief phase of MORB-type volcanism, followed by the purely siliciclastic, turbiditic sediments of the Føssjøen Formation. Sedimentation in the basin was terminated by a tectonic phase that folded the Ilfjellet Group prior to deposition of the unconformably overlying Hovin Group (Fig. 3B).

Source Areas and Maximum Depositional Ages

Detrital zircon spectra are widely used to constrain the nature of source areas and maximum depositional ages of sedimentary successions (e.g., Fedo et al., 2003; Dickinson and Gehrels, 2009; Coutts et al., 2019). Detrital zircon grains are either directly derived from erosion of igneous and metamorphic source rocks, or they represent recycled grains from older sedimentary successions. The detrital zircon spectra from the four samples of the Ilfjellet Group are all characterized by zircons belonging to three age groups: Archean, Paleo-, to Neoproterozoic, and Cambro-Ordovician (Fig. 12).

The Archean zircons (ca. 3200–2400 Ma; up to 21% of the grains; Fig. 12) indicate derivation either from an Archean protosource, or from older sedimentary successions containing a considerable Archean detrital zircon population. Archean detrital zircons are rare in late Mesoproterozoic to late Neoproterozoic sedimentary successions of the Scandinavian Caledonides, Svalbard, Greenland, and the British Isles (e.g., Spencer and Kirkland, 2016), indicating that recycling from only these widely distributed successions cannot explain the presence of this population in our samples. Given the Laurentian affinity of the related Hølonda units, the cratonic parts of Laurentia, or younger cover successions containing abundant Archean detrital zircons such as the Huronian Supergroup (Craddock et al., 2013) or the Stoer Group (Rainbird et al., 2001), are the most probable sources for this population.

The zircons with ages between 2100 and 900 Ma (28%–60% of the grains; Fig. 12) indicate that the Ilfjellet Group sediments were sourced from a composite continental landmass including a variety of Paleo- to Neoproterozoic sources. Such detrital zircons are common in many Proterozoic to Ordovician sedimentary successions of the North Atlantic region, and they are thus of limited use for a source identification (Slagstad and Kirkland, 2017).

Given the geological context, the Cambro-Ordovician zircon grains (500–440 Ma; 34%–59% of the grains) were likely sourced from oceanic

island arcs and ophiolites within the Iapetus Ocean. Indeed, the peaks in zircon ages between 475 and 490 Ma correspond well with the known ages from the LVB and other supra-subduction ophiolites in the Scandinavian Caledonides (e.g., Dunning and Pedersen, 1988; Slagstad et al., 2014). The quartz dioritic clast of the Skjøla olistostrome dated by TIMS (Fig. S2) overlaps in age and composition with the Fagervika granitoid in the LVB, supporting a derivation of some of the detritus from adjacent ophiolitic fragments.

The depositional age of the Ilfjellet Group is constrained by U-Pb TIMS ages of its volcanic units to ca. 474–469 Ma (Fig. 11). Both YSG and YGC 2σ MDA estimates from all detrital zircon samples are younger than these volcanic ages, indicating that they represent erroneously young maximum depositional age estimates. Indeed, each of the four detrital zircon samples contains 5–6 detrital grains <5% discordant with apparent ages younger than the U-Pb TIMS ages of the coeval volcanic rocks (Fig. 12). A feasible explanation for the discrepancy is that these grains experienced lead loss at some later point in the Paleozoic (i.e., during the Scandian orogeny at ca. 420–400 Ma). Due to analytical uncertainties and the limited curvature of the concordia during the Paleozoic, such lead loss does not lead to visibly discordant analyses, as discussed also by Andersen et al. (2019) and Dalslåen et al. (2021). The YPP estimates of ca. 475–485 Ma are in accordance with the volcanic ages as well as with the 478 ± 1 Ma TIMS age of the quartz dioritic clast in the Skjøla olistostrome and are interpreted to represent the most reliable MDA estimates.

Petrogenesis of the Volcanic Rocks of the Ilfjellet Group

The MORB-type Lavas

The composition of basaltic lavas can be used to infer the tectonic setting in which they formed (e.g., Pearce, 2014). A negative Nb-Ta anomaly is generally interpreted as representing a subduction signature and allows a first-order division between subduction-related and subduction-unrelated basalts (Dilek and Furnes, 2014). The Ilfjellet basalts are nearly exclusively MORBs with no significant Nb-Ta anomaly (Figs. 6 and 7).

Five samples have slightly elevated Th/Nb ratios and fall just outside the MORB-OIB Array but still well outside of the fields for typical arc-related magmas. As noted by Pearce and Stern (2006), such transitional geochemical signatures are a distinctive feature of most back-arc basins. However, in such settings this signature is generally predominant, in contrast

to the MORB-dominated signature of the Ilfjellet basalts. E-MORB compositions like those of the Ilfjellet Group are also atypical of back-arc basins (Fig. S4C; Saccani, 2015), but are known from some back-arc basins, e.g., in the Sea of Japan (Pouclet et al., 1995). However, to our knowledge none of these share the peculiar association with enriched rocks comparable to those of the Ilfjellet Th-rich units. Local rhyodacite in the Sea of Japan formed only after back-arc spreading (Pouclet et al., 1995) and is also far less enriched than our Th-rich volcanic rocks.

The five samples with slightly elevated Th/Nb ratios lie on trajectories between D-MORB magmas (lower part of the MORB-OIB Array in Fig. 6C) and the Th-enriched intermediate to felsic volcanic units, and hence could theoretically reflect mixing of these melts. Mixing calculations demonstrate that less than 0.1% addition of Th-rich magma to the MORB-type melts would create trace element patterns and elevated Th/Nb ratios comparable to those of our five samples. However, modeling shows that a small crustal influence from assimilation-fractional crystallization (AFC) processes could also account for trace element patterns and slightly elevated Th/Nb ratios comparable to those of some of the Ilfjellet MORB samples. Notably, AFC processes occur at rifted continental margins, a type of volcanic setting that is commonly dominated by MORB with geochemical signatures typical of deep melting as indicated, e.g., by TiO_2/Yb versus Nb/Yb relationships (Fig. S4B; Pearce, 2014) comparable to the Ilfjellet basalts. AFC processes, with variable interaction of the ascending primary MORB-type melts and crustal or sedimentary material in magma chambers, are therefore considered a more viable model for the erratic and limited occurrence of elevated Th/Nb ratios in our samples.

There has long been a consensus that MORB-type magmas form by melting of a variably depleted or enriched sublithospheric mantle; melting typically being facilitated by adiabatic decompression in upwelling asthenosphere (e.g., Condie, 2016). While D-MORB is formed from relatively high degrees of melting of the depleted upper-mantle reservoir depleted MORB mantle (DMM), the origin of incompatible element-enriched E-MORB and OIB is more controversial (Waters et al., 2011; Niu and O'Hara, 2003). Various models for the formation of E-MORB invoke, e.g., mantle heterogeneities or deeper melting in the presence of residual garnet, in contrast to shallow melting of more homogeneous DMM in D-MORB formation (Pearce, 2014).

Large variations in incompatible trace element spectra, as reflected by LREE/HREE and Th/Yb ratios in the Ilfjellet Group MORB (Fig. 7; Table S1), cannot form by crystal fractionation but may be explained in terms of either large variations in degree of partial melting or melting from different sources (e.g., Gale et al., 2013). Systematic covariation of Nd isotope values with MORB type (Fig. 10C) demonstrates that differences in mantle source were the main cause of variations in incompatible-element ratios. Isotopic values of the early, most depleted D-MORB are similar to those of DMM, whereas late E-MORB is comparable to OIB, the latter magma type inferably formed by plume melting at greater mantle depth (Pearce, 2014). This is in accordance with the geochemistry of some enriched MORB samples (Fig. S4B) that implies deep melting. It is noteworthy that the relatively high Sm/Yb ratios (Table S1) of the Ilfjellet D- and T-MORB also suggest some influence of garnet in the mantle source (Niu et al., 2001; Saccani et al., 2008; Wood et al., 2013). This also points to a mantle source region deeper than that of normal mid-ocean ridge settings for the D- and T-MORBs.

The progression of compositions from D- to E-MORB through the stratigraphic succession (Fig. 3) indicates a systematic change in source contribution, with generally increasing input from deeper melting of a less depleted mantle through the limited time interval represented by the Ilfjellet Group. This is consistent with emergent rifting, in contrast to steady-state spreading where a homogeneous shallow melting regime will likely persist. The evolved nature of the majority of Ilfjellet MORBs (e.g., ferrobasaltic and low Mg#) indicates that fractional crystallization played a major role, probably related to shallow magma chambers and high eruption frequency (Natland, 1980; Rubin et al., 2009).

The Th-rich Units

The Th-rich units of the Mostadmarka and Fjellvollen formations show remarkably different trace element patterns and ratios compared to the MORBs, and a common parental magma with the basaltic rocks can be disregarded. While intermediate and felsic rocks are predominant, mafic members exist in at least the Gragjelfjellet, Slættesberget, and Bolhøgdin units (Fig. 6A). This excludes an origin by partial melting of continental crust or terrigenous sediments, which would create only felsic and intermediate melts. The sporadic high contents of Cr, Ni, Co, and MgO (Fig. 8) also point to a mantle rather than a crustal source region, possibly reflecting an erratic occurrence of trapped mantle xenocrysts. The considerable differences between the individual Th-rich units indicate that they were derived from at least three different magma sources.

Within the different Th-rich units, roughly parallel trace element and REE patterns, as well as gradually decreasing TiO_2 and P_2O_5 and increasingly negative Eu anomalies with increasing SiO_2 (Figs. 8 and 9), indicate that fractional crystallization from mafic parental magma(s) might have occurred, with removal of Fe-Ti oxides, apatite, and feldspar. The general enrichment of some highly incompatible elements, such as Th, with increasing SiO_2 in the Gragjelfjellet unit (Fig. 6A) is consistent with fractional crystallization for that unit. By contrast, the Bolhøgdin unit shows no enrichment of Th with increasing SiO_2 (Fig. 6A). Scatter of other incompatible trace elements with SiO_2 (Fig. 8) also argues against simple fractionation. Moreover, the general predominance of intermediate and felsic over mafic rocks in the Th-rich units is seemingly at odds with a model of fractional crystallization from parental mafic magmas, where SiO_2-rich differentiates would likely be volumetrically subordinate.

A more conceivable model is that of combined fractional crystallization of a mafic parental magma and associated assimilation (AFC), especially in case of interaction with continental crust (average continental crust: 5.6 ppm Th and 60.6 wt% SiO_2; Rudnick and Gao, 2003), which may strongly affect SiO_2 without increasing the concentrations of highly incompatible elements; Nd and Sr isotopic signatures would also not be significantly affected if the isotopic compositions of the primary magmas and assimilated crust were broadly similar.

Volcanic rocks with similarly enriched trace element and REE characteristics are relatively rare, and have not previously been reported from the Caledonian orogenic belt except in correlative units farther south in the Trondheim Nappe Complex (Dalslåen et al., 2020a, 2020b). Their overall geochemical characteristics, with Nb, Ta, and Ti depletion and Pb enrichment (Fig. 9), show some affinity to subduction-related rocks, but they are far more enriched in elements like Th, U, LREE, and Zr even when compared with continental arcs. Also, their high concentrations of elements like Be, Sn, and W are more suggestive of late- to post-orogenic and intracratonic settings (Ryan, 2002; Dailey et al., 2018; Hulsbosch, 2019; Lehmann, 2021).

A rigorous geochemical comparison with volcanic rocks of known, relatively young (Cenozoic) geotectonic settings in the GEOROC database shows that comparable trace element and REE patterns are relatively rare also in modern settings, and are essentially restricted to orogens such as the Alpine-Himalayan belt and, in particular, the circum-Tyrrhenian region of the Mediterranean, where ultrapotassic rocks are strikingly similar to those of the Ilfjellet Th-rich units (Fig. 13). In these settings, such rocks are generally interpreted in terms of a complex
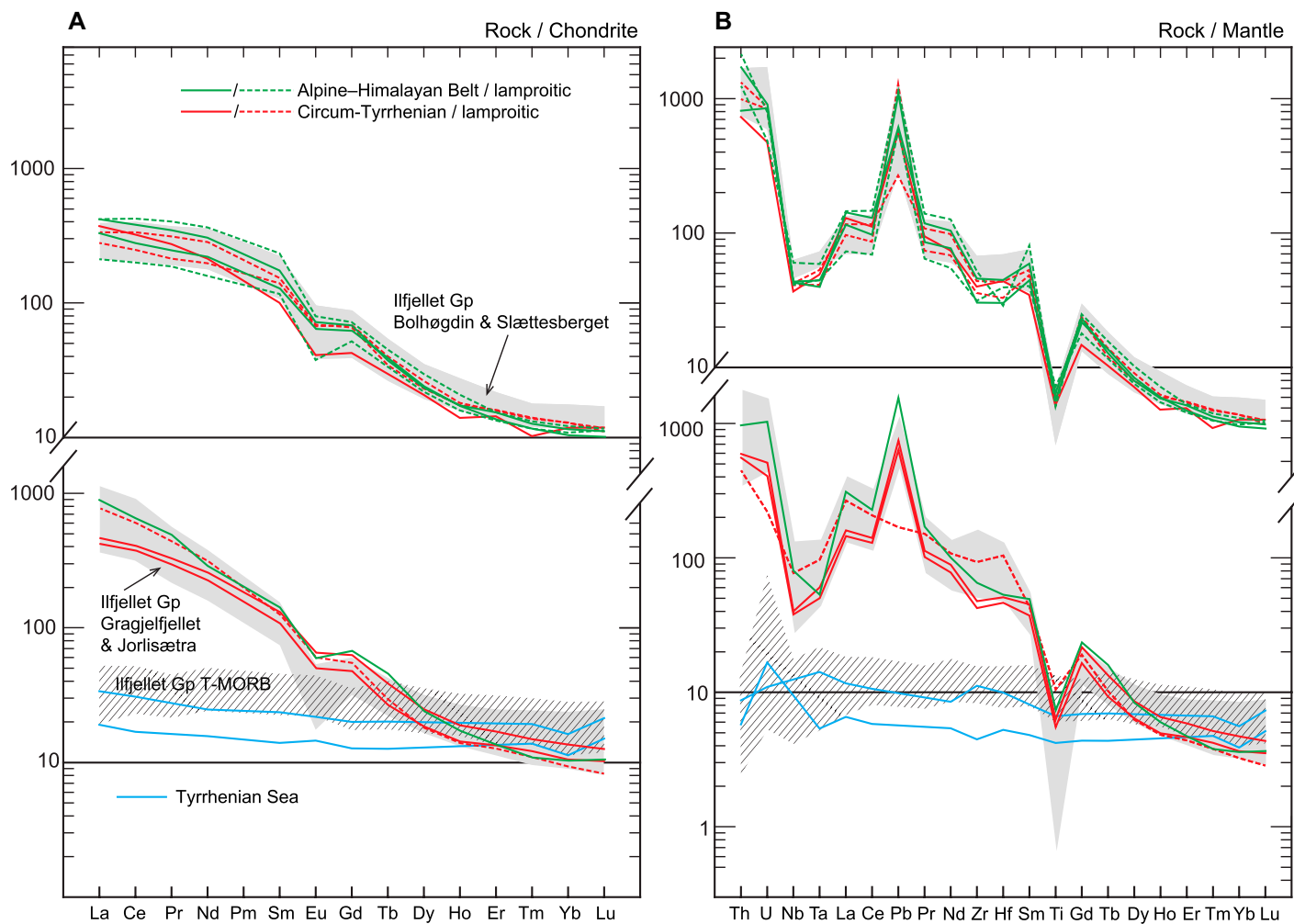
Figure 13. Geochemical comparison of volcanic rocks from the Ilfjellet Group (Gp) (Fig. 2) (gray shaded fields) and ultrapotassic volcanic rocks from the Alpine-Himalayan Belt (green lines) and the circum-Tyrrhenian igneous provinces of the Mediterranean (red lines). Two mid-ocean ridge basalts (MORB) from the Tyrrhenian Sea are included for comparison with the Ilfjellet Group transitional (T)-MORBs (hatched field). Selected samples; Conticelli et al. (2009): MVC100, VS29, and VS202 (all Tuscany, Italy), SIS4 (Corsica); Conticelli et al. (2010): VS232 (Tuscany), WAOSavb (Western Alps); Guo et al. (2015): BG203 and SQH-08 (both Tibet); Zhao et al. (2009): SL0625 (Tibet); Barberi et al. (1978): 2-1, 136-142, and 7-4, 130-135 (both Tyrrhenian basin).

polyphase genesis involving subduction of continental material, metasomatism of the overlying lithospheric mantle, and melting of metasomatized mantle domains during postorogenic extension (Foley, 1992; Peccerillo, 1999; Conticelli et al., 2009; Prelević et al., 2008; Cheng and Guo, 2017). Volcanic rocks that have the peculiar, upward-convex LREE patterns typical of the Bolhøgdin and Slættesberget units are quite common in such settings (Fig. 13A); the majority of these are lamproitic, but transitional types with higher Al_2O_3, approaching the geochemical characteristics of Foley's (1992) Group III ultrapotassic rocks (Roman Province Type), also exist (Gao et al., 2007; Conticelli et al., 2010; Guo et al., 2015).

Based on these similarities, we envisage a petrogenetic model for the evolution of the Th-rich

units of the Ilfjellet, Kinna, and Trollhøtta rocks analogous to that in the younger orogenic or postorogenic settings. We interpret the parental, mafic magmas as being derived from highly enriched, lithospheric mantle domains that had been previously metasomatized by fluids and melts from subducted continental material. The coexistence of these Th-rich rocks with the MORB-type basalts demonstrates that the Ilfjellet volcanism was concurrently tapping distinctly different mantle sources, namely asthenospheric, normal MORB mantle (including DMM) as well as strongly enriched lithospheric mantle domains. The relatively high Al_2O_3 of our rocks is interpreted in terms of a lherzolitic mantle source, in contrast to lamproitic magmas that are thought to be derived from harzburgitic mantle (Bergman, 1987). We also speculate that sig-

nificant negative Eu anomalies even in the least evolved, mafic varieties stem from a metasomatized mantle that had acquired a Eu anomaly from crustal or sedimentary sources.

## Tectonic Setting of the Ilfjellet Group

Arc-Continent Collision, Polarity Flip, and Slab Rollback

Plate tectonic reconstructions show that formation of the Ilfjellet Group at 475–463 Ma occurred in an overall convergent tectonic setting within the Iapetus realm. Convergence dominated between Gondwana and Laurentia since at least ca. 500 Ma and between Baltica and Laurentia since at least 480 Ma (Fig. 14A; Domeier, 2016). There was a particular increase in convergence rate of Baltica toward Laurentia
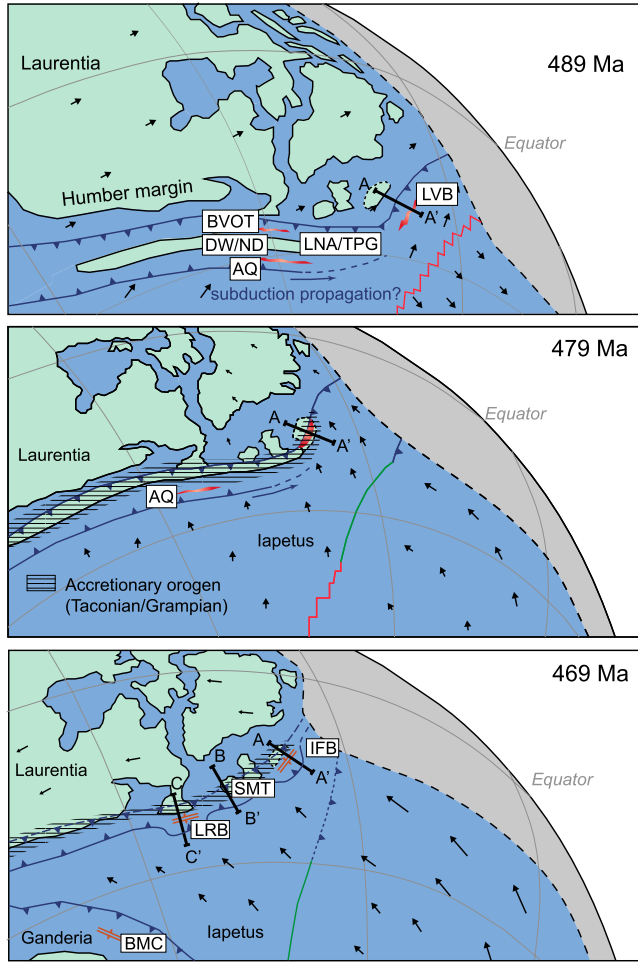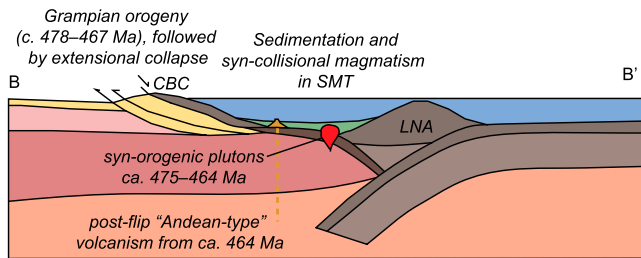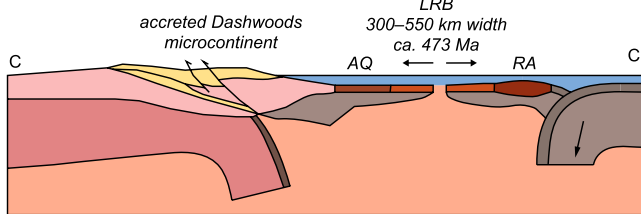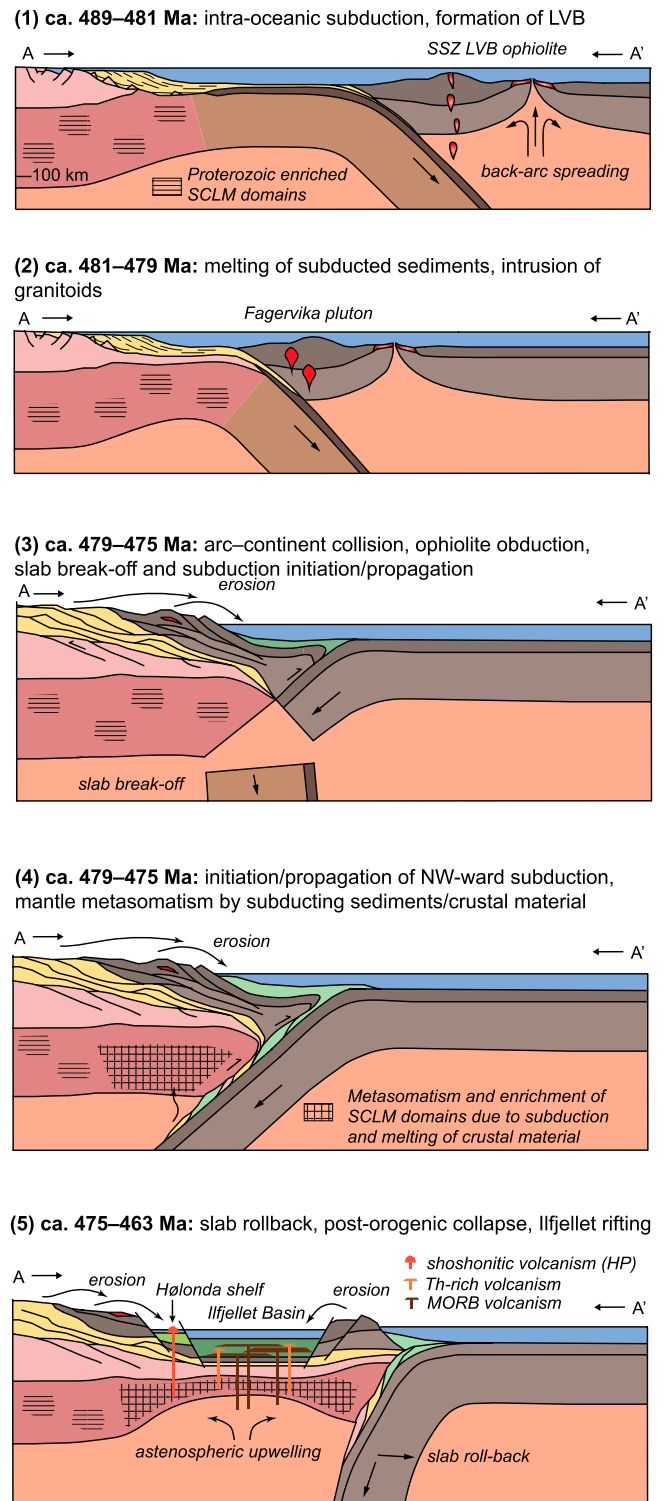
Figure 14. Tectonic interpretation for the Ilfjellet basin (including the Klæbu, Jonsvatnet, Mostadmarka, Fjellvollen and Føssjøen formations, Fig. 2) from ca. 489–463 Ma along the Laurentian margin. For details, see text. AQ—Annieopsquotch ophiolite belt; BMC—Bathurst Mining Camp; BVOT—Baie Verte Oceanic Tract; CBC—Clew Bay Complex; DW—Dashwood microcontinent; HP—Hølonda Porphyrites; IFB—Ilfjellet basin; LNA—Lough Nafooey Arc; LRB—Lloyds River basin; LVB—Løkken-Vassfjellet-Bymarka ophiolite; ND—Notre Dame Arc; RA—Roberts Arm Arc; SCLM—subcontinental lithospheric mantle; SMT—South Mayo Trough; TPG—Tyrone Plutonic Group.

at 480–470 Ma, implying that intra-oceanic and continental-margin tectonics were dominated by subduction-zone dynamics (Domeier, 2016).

Formation of the Ilfjellet basin was preceded by the formation of the LVB ophiolites that are generally considered to be remnants of a 487–480 Ma oceanic back-arc basin above a southeast-vergent subduction zone (Fig. 14B-1; Grenne et al., 1999; Slagstad et al., 2014). Intrusion of the Fagervika granitoid at 481 Ma has been interpreted to reflect partial melting of terrigenous sediments as the continental margin was approaching the trench (Fig. 14B-2; Slagstad et al., 2014). Shortly after, the arc–back-arc complex collided with the continental margin and the ophiolite was obducted, uplifted and exposed to erosion; the 478 ± 1 Ma age of a quartz dioritic clast in the Skjøla olistostrome limits the time for ophiolite obduction to after 479 Ma (Fig. 14B-3).

Arc-continent collision and ophiolite obduction must have been followed by slab break-off (Fig. 14B-3), and a subsequent shift to northwest-vergent subduction as evidenced by late Ordovician to Silurian batholiths that were emplaced in Laurentian margin terranes elsewhere in Norway (Barnes et al., 2007; Augland et al., 2012). This could occur either by compression-induced subduction initiation (Stern and Gerya, 2018) due to the arrival of buoyant lithosphere at the former trench outboard of the arc-continent collision zone, or by along-strike propagation (Zhou et al., 2020) of a pre-existing continent-dipping subduction zone from farther south (Fig. 14A).

The newly-formed trench obviously received considerable detritus from the exhumed arc-continent collision zone, leading to excessive sediment input to the down-going slab (Fig. 14B-3). Partial melting of this continental detritus and crustal material from subduction erosion produced metasomatic enrichment in the overlying, thick subcontinental lithosphere below the arc-continent collision zone (Fig. 14B-4). Postorogenic collapse, facilitated by slab rollback, led to extensional thinning of the overlying lithosphere and to associated subsidence and sedimentation in the Ilfjellet basin (Fig. 14B-5).

The evolution from D-MORB to E-MORB basalts in the Ilfjellet basin indicates that magmatism initially tapped asthenospheric DMM mantle and gradually involved deeper, less depleted mantle as a result of asthenospheric upwelling associated with rollback. Further, this upwelling led to heating and partial melting of metasomatized lithospheric mantle domains and triggered eruption of the Th-rich, at least partly ultrapotassic, magmas (Fig. 14B-5). In such a setting, the shoshonitic Hølonda Porphyrites could represent partial melting of lithospheric mantle domains less enriched by metasomatic

processes (Dalslåen et al., 2020b), implying that they were not necessarily related to Andean-type oceanic subduction as proposed earlier (Grenne and Roberts, 1998; Hollocher at al., 2016).

Mesoproterozoic to early Neoproterozoic Nd model ages (Fig. 10B) constrain possible sources for the enrichment in the Th-rich units. The apparently most viable model includes subducted sediments and continental margin crust, which metasomatized the overlying lithospheric mantle wedge during early stages of the northwest-vergent subduction (Fig. 14B-4). It is also possible that mantle enrichment had been acquired already during Proterozoic accretionary orogenies (Fig. 14B-1; Condie, 2013); seismic tomographic evidence suggests that such refertilized mantle still exists under the eastern North American craton edge (Boyce et al., 2016).

Along-Strike Variations at the Laurentian Margin

Broadly comparable tectonic processes, with obduction and/or accretion of various oceanic complexes followed by subduction polarity flip, have been identified along the entire Laurentian margin during the ca. 490–460 Ma time interval (Fig. 14A-C; Ryan and Dewey 1991, 2011; Dewey, 2005; Draut et al., 2009; van Staal et al., 2009; Cooper et al., 2011; Zagorevski and van Staal, 2011; Hollis et al., 2012). The polarity reversal, possibly facilitated by northward propagation of a pre-existing northwest-dipping subduction zone, was accompanied by the formation of a series of different volcano-sedimentary basins all along the margin.

Several of these basins overlap in age with the Ilfjellet Group, such as the ca. 475 Ma Tyrone Volcanic Group in central Ireland (Cooper et al., 2011; Hollis et al., 2012), the 475–470 Ma Tourmakeady Volcanic Group of the South Mayo Trough in western Ireland (Fig. 14C; Ryan and Dewey, 2011), and the ca. 473 Ma Lloyds River back-arc basin of Newfoundland (Fig. 14D; Zagorevski et al., 2006, 2009). Parts of the Tetagouche, Fournier, and California Lake groups of the Bathurst Mining Camp area are of similar age (ca. 475–470 Ma) but belong to the Gander terrane located considerably outboard of the Laurentian margin at the time of formation (Figs. 1 and 14A; van Staal et al., 1991; Rogers and van Staal, 2003). Associations of MORB-type basalts and felsic volcanic rocks are known from these basins; however, a detailed analysis of documented geochemistry and stratigraphic relationships shows that none of these basins exhibit intimate associations of MORB and extremely enriched, originally ultrapotassic volcanic rocks comparable to those of the Ilfjellet basin. This indicates that along-strike variations in the geometry of the continental margin and

the nature of the colliding oceanic terranes, as well as processes associated with subduction initiation and/or propagation (e.g., rollback and formation of curved subduction zones; Brown et al., 2011) have contributed to unique basins with individual volcano-sedimentary histories along the entire margin.
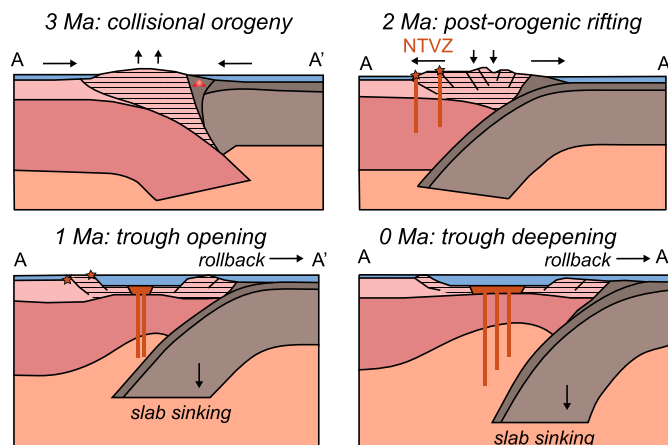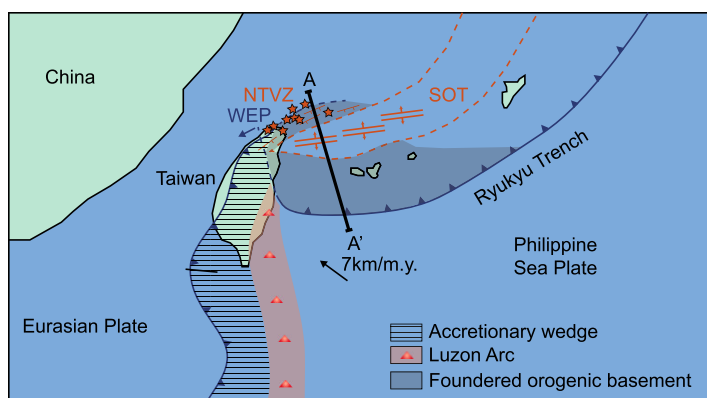
Possible Modern Analogues

To our knowledge, an intimate association of MORB and extremely enriched, originally ultrapotassic volcanic rocks as observed in the Ilfjellet basin has not been documented within the same stratigraphic succession neither in ancient nor in modern settings. Nevertheless, broad similarities in petrological and plate tectonic development with the Taiwan-Ryukyu region and the Tyrrhenian region in the Mediterranean may shed some light on the origin of the Ilfjellet basin (Fig. 15).

The Taiwan region is generally described as a modern example of arc-continent collision. A pre-existing subduction zone (the Ryukyu subduction zone) is propagating laterally southwards and underthrusts the collision zone, possibly leading to future polarity reversal (Fig. 15A; Teng, 1990, 1996; Clift et al., 2003). In the transitional region between arc-continent collision and the underthrusting Philippine Sea Plate, extensional collapse and subsidence are associated with subordinate ultrapotassic volcanism in the Northern Taiwan volcanic zone (NTVZ) and basaltic volcanism in the Southern Okinawa Trough (SOT) (Fig. 15A; Teng, 1996; Wang et al., 1999, 2004; Shinjo et al., 1999). Although the NTVZ magmas are far less enriched than our Th-rich units, and the SOT basalts have distinct arc or back-arc basin signatures in contrast to the Ilfjellet MORBs, the southward propagation of subduction of the Philippine Sea Plate might be a possible tectonic analogue for the inferred northward along-strike propagation of a continent-directed subduction zone along the Laurentian margin from ca. 480 Ma onwards (Fig. 14A).

The Tyrrhenian region comprises coeval MORB and highly enriched rocks similar to those of the Ilfjellet basin, although the contrasting magma types have not yet been documented within the same stratigraphic succession (Figs. 13 and 15B). Situated within an overall convergent setting between Africa and Europe, the Tyrrhenian Sea opened from ca. 10 Ma onwards, as represented by 7.3–4.3 Ma MORB-type basalts of the Vavilov basin (Fig. 15B; Peccerillo, 2005). The Tyrrhenian Sea is flanked on both sides by volcanic provinces with potassic to ultrapotassic rocks (Figs. 13 and 15B; Conticelli et al., 2010). Initial southward subduction of the European continent below the Adriatic microcontinent, including the obduction of

A Taiwan: subduction polarity flip and opening of the Southern Okinawa Through (3–0 Ma)

B Mediterranean: subduction polarity flip and opening of the Tyrrhenian basin (10–0 Ma)
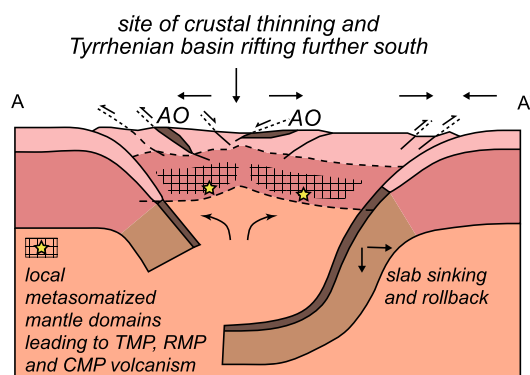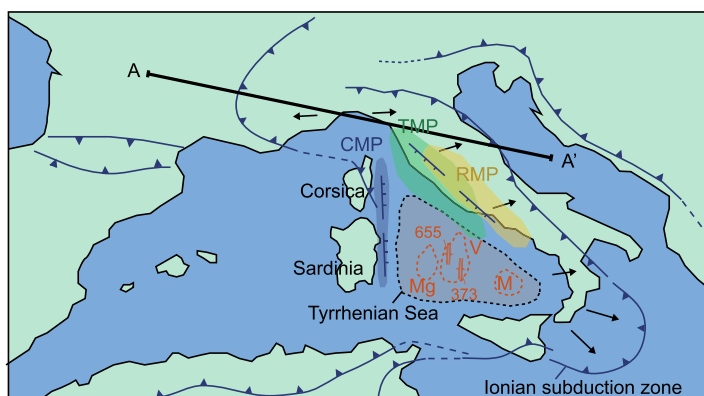
Figure 15. Possible modern analogues for the tectonic setting of the Ilfjellet basin (Fig. 2). (A) the Taiwan-Ryukyu system along the western margin of the Pacific. (B) The Tyrrhenian region of the Mediterranean. For details, see text. AO—Alpine ophiolites; CMP—Corsican Magmatic Province; M—Marsili Basin; Mg—Magnaghi Basin; NTVZ—Northern Taiwan volcanic zone; RMP—Roman Magmatic Province; SOT—Southern Okinawa Trough; TMP—Tuscan Magmatic Province; V—Vasilov Basin; WEP—Western Plate Boundary.

ophiolites, was followed by northward subduction along the Ionian subduction system, which subsequently retreated, rotated, and opened the Tyrrhenian Sea (Fig. 15B; Royden, 1993; Vignaroli et al., 2008; Rosenbaum, 2014; Mantovani et al., 2020).

The Tyrrhenian Sea represents an anomaly with its upwelling asthenospheric mantle in a region of relatively thick orogenic lithosphere (e.g., Finetti et al., 2001; Cella et al., 2006; Di Stefano et al., 2009). The geochemical character of its MORB-type basalts demonstrates that asthenospheric melts can reach the seafloor in localized basins without significant crustal contamination even in regions dominated by previously thickened lithosphere, similar to our observations from the Ilfjellet basin.

We envisage a tectonic scenario for the development of the Ilfjellet basin along the Early- to Mid-Ordovician Laurentian margin (Fig. 14B)

broadly similar to the Taiwan-Ryukyu or Tyrrhenian settings (Fig. 15). Whether the Ilfjellet setting was relatively linear such as the Taiwan-Ryukyu system, or included a significant rotational component such as the Tyrrhenian system, is difficult to constrain since the original along-strike extent is unknown and the original geometry was highly distorted during the later continent-continent collision.

CONCLUSIONS

Our results show that what has previously been referred to as the Støren Group in the central Scandinavian Caledonides consists of two distinctly different geological units: (1) the northwestern, ca. 489–480 Ma, Løkken-Vassfjellet-Bymarka (LVB) ophiolite, and (2) the unconformably overlying, ca. 475–463 Ma, Ilfjellet Group. In order to avoid future confusion

between the two, we suggest abandoning the term Støren Group entirely.

The Ilfjellet Group consists of turbidite-dominated formations (Klæbu, Fjellvollen, and Føssjøen formations), intercalated with mainly basalt-dominated successions (Jonsvatnet and Mostadmarka formations). The basalts show a transition from D- to E-MORB compositions stratigraphically upward, indicating melt derivation from an increasingly deeper asthenospheric mantle source. We identified five volcanic units with extreme enrichments in Th and other highly incompatible trace elements: the Gragjelfjellet (473 ± 1 Ma), Slættesberget, Vertjønna, Jorlisætra (473 ± 1 Ma), and Bolhøgdin units (470 ± 1 Ma). These units are interpreted to represent partly ultrapotassic melts derived from metasomatically enriched lithospheric mantle. To our knowledge, the intimate association of MORB with such extremely enriched rocks has

not been documented elsewhere, neither within the Iapetus realm of the Caledonian-Appalachian orogen nor in modern settings.

We interpret the Ilfjellet Group to have formed in an extensional basin that developed along the Laurentian margin from ca. 475 Ma to ca. 463 Ma, subsequent to arc-continent collision and ophiolite obduction. Rifting and subsidence was related to postorogenic collapse facilitated by slab rollback of an outboard, newly initiated or laterally northwards-propagating, continent-dipping subduction zone. The Taiwan-Ruyku system or the Tyrrhenian region of the Mediterranean, both characterized by the close geographic proximity of MORB-type and ultrapotassic volcanic rocks, may represent modern examples of tectonic settings broadly similar to that of the Ilfjellet basin.

ACKNOWLEDGMENTS

REFERENCES CITED

Acocella, V., 2019, Bridging the gap from caldera unrest to resurgence: Frontiers in Earth Science, v. 7, p. 1–7, https://doi.org/10.3389/feart.2019.00173.

Allen, S.R., Fiske, R.S., and Tamura, Y., 2010, Effects of water depth on pumice formation in submarine domes at Sumisu, Izu-Bonin arc, western Pacific: Geology, v. 38, p. 391–394, https://doi.org/10.1130/G30500.1.

Andersen, T., Elburg, M.A., and Magwaza, B.N., 2019, Sources of bias in detrital zircon geochronology: Discordance, concealed lead loss and common lead correction: Earth-Science Reviews, v. 197, no. 102899, https://doi.org/10.1016/j.earscirev.2019.102899.

Augland, L.E., Andresen, A., and Corfu, F., 2010, Age, structural setting, and exhumation of the Liverpool Land eclogite terrane, East Greenland Caledonides: Lithosphere, v. 2, p. 267–286, https://doi.org/10.1130/L75.1.

Augland, L.E., Andresen, A., Corfu, F., Simonsen, S., and Andersen, T., 2012, The Beiarn Nappe Complex: A record of Laurentian Early Silurian arc magmatism in the Uppermost Allochthon, Scandinavian Caledonides: Lithos, v. 146–147, p. 233–252, https://doi.org/10.1016/j.lithos.2012.05.016.

Ballo, E.G., Augland, L.E., Hammer, Ø., and Svensen, H., 2019, A new age model for the Ordovician (Sandbian) K-bentonites in Oslo, Norway: Palaeogeography, Palaeoclimatology, Palaeoecology, v. 520, p. 203–213, https://doi.org/10.1016/j.palaeo.2019.01.016.

Barberi, F., Bizouard, H., Capaldi, G., Ferrara, G., Gasparini, P., Innocenti, F., Joron, J.L., Lambert, B., Treuil, M., and Allegre, C., 1978, Age and nature of basalts from the Tyrrhenian Abyssal Plain, in Hsu, K., Montadert, L., et al., eds., Initial Reports of the Deep Sea Drill-ing Project, v. 42, p. 509–514, https://doi.org/10.2973/dsdp.proc.42-1.118.1978.

Barnes, C.G., Frost, C.D., Yoshinobu, A.S., McArthur, K., Barnes, M.A., Allen, Ch.M., Nordgulen, Ø., and Prestvik, T., 2007, Timing of sedimentation, metamorphism, and plutonism in the Helgeland Nappe Complex, north-central Norwegian Caledonides: Geosphere, v. 3, p. 683–703, https://doi.org/10.1130/GES00184.1.

Bergman, S.C., 1987, Lamproites and other potassium-rich igneous rocks: A review of their occurrence, mineralogy and geochemistry, in Fitton, J.G., and Upton, B.G.J., eds, Alkaline Igneous Rocks: Geological Society Special Publication, v. 30, p. 103–190, https://doi.org/10.1144/GSL.SP.1987.030.01.08.

Boyce, A., Bastow, I.D., Darbyshire, F.A., Ellwood, A.G., Gilligan, A., Levin, V., and Menke, W., 2016, Subduction beneath Laurentia modified the eastern North American cratonic edge: Evidence from P wave and S wave tomography: Journal of Geophysical Research. Solid Earth, v. 121, p. 5013–5030, https://doi.org/10.1002/2016JB012838.

Brown, D., Ryan, P.D., Afonso, J.C., Boutelier, D., Burg, J.P., Byrne, T., Calvert, A., Cook, F., DeBari, S., and Dewey, J.F., 2011, Arc-continent collision: The making of an orogen, in Brown, D., and Ryan, P.D., eds., Arc-Continent Collision: Frontiers in Earth Sciences: Berlin, Heidelberg, Germany, Springer, p. 477–493, https://doi.org/10.1007/978-3-540-88558-0_17.

Bruton, D.L., and Bockelie, J.F., 1980, Geology and paleontology of the Hølonda area, western Norway: A fragment of North America? in Wones, D.R., ed., The Caledonides in the USA: Virginia Polytechnic Geological Sciences Memoir, v. 2, p. 41–55.

Burke, K., Dewey, J.F., and Kidd, W.S.F., 1977, World distribution of sutures: The sites of former oceans: Tectonophysics, v. 40, p. 69–99, https://doi.org/10.1016/0040-1951(77)90030-0.

Busby, C., 2005, Possible distinguishing characteristics of very deepwater explosive and effusive silicic volcanism: Geology, v. 33, p. 845–848, https://doi.org/10.1130/G21216.1.

Carey, R., Soule, S.A., Manga, M., White, J.D.L., McPhie, J., Wysoczanski, R., Jutzeler, M., Tani, K., Yoerger, D., Fornari, D., Tontini, F.C., Houghton, B., Mitchell, S., Ikegami, F., Conway, C., Murch, A., Fauria, K., Jones, M., Cahalan, R., and McKenzie, W., 2018, The largest deep-ocean silicic volcanic eruption of the past century: Science Advances, v. 4, no. 1, https://doi.org/10.1126/sciadv.1701121.

Cella, F., de Lorenzo, S., Fedi, M., Loddo, M., Mongelli, F., Rapolla, A., and Zito, G., 2006, Temperature and density of the Tyrrhenian lithosphere and slab and new interpretation of gravity field in the Tyrrhenian Basin: Tectonophysics, v. 412, p. 27–47, https://doi.org/10.1016/j.tecto.2005.08.025.

Cheng, Z., and Guo, Z., 2017, Post-collisional ultrapotassic rocks and mantle xenoliths in the Sailipu volcanic field of Lhasa terrane, south Tibet: Petrological and geochemical constraints on mantle source and geodynamic setting: Gondwana Research, v. 46, p. 17–42, https://doi.org/10.1016/j.gr.2017.02.008.

Clift, P.D., Schouten, H., and Draut, A.E., 2003, A general model of arc-continent collision and subduction polarity reversal from Taiwan and the Irish Caledonides, in Larter, R.D. and Leat, P.T., eds., Intra-Oceanic Subduction Systems: Tectonic and Magmatic Processes: Geological Society of London, Special Publication 219, p. 81–98, https://doi.org/10.1144/GSL.SP.2003.219.01.04.

Clift, P.D., Dewey, J.F., Draut, A.E., Chew, D.M., Mange, M., and Ryan, P.D., 2004, Rapid tectonic exhumation, detachment faulting and orogenic collapse in the Caledonides of western Ireland: Tectonophysics, v. 384, p. 91–113, https://doi.org/10.1016/j.tecto.2004.03.009.

Condie, K., 2013, Preservation and recycling of crust during accretionary and collisional phases of Proterozoic orogens: A bumpy road from Nuna to Rodinia: Geosciences, v. 3, p. 240–261, https://doi.org/10.3390/geosciences3020240.

Condie, K.C., 2016, Earth as an Evolving Planetary System: Cambridge, Massachusetts, USA, Academic Press, 430 p., https://doi.org/10.1016/C2015-0-00179-4.

Conticelli, S., Guarnieri, L., Farinelli, A., Mattei, M., Avanzinelli, R., Bianchini, G., Boari, E., Tommasini, S., Tiepolo, M., Prelevic, D., and Venturelli, G., 2009, Trace elements and Sr-Nd-Pb isotopes of K-rich, shoshonitic, and calc-alkaline magmatism of the Western Mediterranean Region: Genesis of ultrapotassic to calc-alkaline magmatic associations in a post-collisional geodynamic setting: Lithos, v. 107, p. 68–92, https://doi.org/10.1016/j.lithos.2008.07.016.

Conticelli, S., Laurenzi, M.A., Giordano, G., Mattei, M., Avanzinelli, R., Melluso, L., Tommasini, S., Boari, E., Cifelli, F., and Perini, G., 2010, Leucite-bearing (kamafugitic/leucititic) and -free (lamproitic) ultrapotassic rocks and associated shoshonites from Italy: Constraints on petrogenesis and geodynamics, in Beltrando, M., Peccerillo, A., Mattei, M., Conticelli, S., and Doglioni, C., eds., Journal of the Virtual Explorer, v. 36, paper 20, https://doi.org/10.3809/jvirtex.2010.00251.

Cooper, M.R., Crowley, Q.G., Hollis, S.P., Noble, S.R., Roberts, S., Chew, D., Earls, G., Herrington, R., and Merriman, R.J., 2011, Age constraints and geochemistry of the Ordovician Tyrone Igneous Complex, Northern Ireland: Implications for the Grampian orogeny: Journal of the Geological Society, v. 168, p. 837–850, https://doi.org/10.1144/0016-76492010-164.

Coutts, D.S., Matthews, A., and Hubbard, S.M., 2019, Assessment of widely used methods to derive depositional ages from detrital zircon populations: Geoscience Frontiers, v. 10, p. 1421–1435, https://doi.org/10.1016/j.gsf.2018.11.002.

Covault, J.A., 2011, Submarine fans and canyon-channel systems: A review of processes, products, and models: Nature Education Knowledge, v. 3, no. 10, https://www.nature.com/scitable/knowledge/library/submarine-fans-and-canyon-channel-systems-a-24178428.

Craddock, J.P., Rainbird, R.H., Davis, W.J., Davidson, C., Vervoort, J.D., Konstantinou, A., Boerboom, T., Vorhies, S., Kerber, L., and Lundquist, B., 2013, Detrital zircon geochronology and provenance of the Paleoproterozoic Huron (∼2.4–2.2 Ga) and Animikie (∼2.2–1.8 Ga) basins, southern Superior Province: The Journal of Geology, v. 121, p. 623–644, https://doi.org/10.1086/673265.

Dailey, S.R., Christiansen, E.H., Dorais, M.J., Kowallis, B.J., Fernandez, D.P., and Johnson, D.M., 2018, Origin of the fluorine- and beryllium-rich rhyolites of the Spor Mountain Formation, Western Utah: The American Mineralogist, v. 103, p. 1228–1252, https://doi.org/10.2138/am-2018-6256.

Dalslåen, B.H., Gasser, D., Grenne, T., Augland, L.E., and Andresen, A., 2020a, Early to Middle Ordovician sedimentation and bimodal volcanism at the margin of Iapetus: The Trollhøtta-Kinna basin of the Central Norwegian Caledonides, in Murphy, J., Strachan, R., and Quesada, C., eds., Pannotia To Pangaea: Neoproterozoic and Paleozoic Orogenic Cycles in the Circum-Atlantic Region: Geological Society of London, Special Publication 503, p. 251–277, https://doi.org/10.1144/SP503-2020-37.

Dalslåen, B.H., Gasser, D., Grenne, T., Augland, L.E., and Corfu, F., 2020b, Ordovician shoshonitic to ultrapotassic volcanism in the central Norwegian Caledonides: The result of sediment subduction, mantle metasomatism and mantle partial melting: Lithos, v. 356, no. 105372, https://doi.org/10.1016/j.lithos.2020.105372.

Dalslåen, B.H., Gasser, D., Grenne, T., Ganerød, M., and Andresen, A., 2021, The Skuggliberga unit of the Oppdal area, central Scandinavian Caledonides: Calc-alkaline pyroclastic volcanism in a fluvial to shallow marine basin following a mid-Ordovician orogenic event: Norsk Geologisk Tidsskrift, https://doi.org/10.17850/njg101-2-2.

de Wit, M.J., Linol, B., Furnes, H., Muedi, T., and Valashiya, K., 2020, Pillow talk: Volcanic rocks of the Karoo that formed many leagues under the Gondwanan Sea: South African Journal of Geology, v. 123, p. 297–330, https://doi.org/10.25131/sajg.123.0021.

Dewey, J.F., 2005, Orogeny can be very short: Proceedings of the National Academy of Sciences of the United States of America, v. 102, p. 15286–15293 https://doi.org/10.1073pnas.0505516102, https://doi.org/10.1073/pnas.0505516102.

Dickinson, W.R., and Gehrels, G.E., 2009, Use of U-Pb ages of detrital zircons to infer maximum depositional ages of strata: A test against a Colorado Plateau Mesozoic database: Earth and Planetary Science Letters, v. 288, p. 115–125, https://doi.org/10.1016/j.epsl.2009.09.013.

Dilek, Y., and Furnes, H., 2014, Ophiolites and their origins: Elements, v. 10, p. 93–100, https://doi.org/10.2113/gselements.10.2.93.

Di Stefano, R., Kissling, E., Chiarabba, C., Amato, A., and Giardini, D., 2009, Shallow subduction beneath Italy: Three-dimensional images of the Adriatic-European-Tyrrhenian lithosphere system based on high-quality P wave arrival times: Journal of Geophysical Research. Solid Earth, v. 114, no. B5, https://doi.org/10.1029/2008JB005641.

Di Vito, M., Acocella, V., Aiello, G., Barra, D., Battaglia, M., Carandente, A., Del Gaudio, C., de Vita, S., Ricciardi, G.P., Ricco, C., Scandone, R., and Terrasi, F., 2016, Magma transfer at Campi Flegrei caldera (Italy) before the 1538 AD eruption: Scientific Reports, v. 6, no. 32245, https://doi.org/10.1038/srep32245.

Domeier, M., 2016, A plate tectonic scenario for the Iapetus and Rheic oceans: Gondwana Research, v. 36, p. 275–295, https://doi.org/10.1016/j.gr.2015.08.003.

Draut, A.E., Clift, P.D., Amato, J.M., Blusztajn, J., and Schouten, H., 2009, Arc-continent collision and the formation of continental crust: A new geochemical and isotopic record from the Ordovician Tyrone Igneous Complex, Ireland: Journal of the Geological Society, v. 166, p. 485–500, https://doi.org/10.1144/0016-76492008-102.

Dunning, G.R., and Pedersen, R.B., 1988, U/Pb ages of ophiolites and arc-related plutons of the Norwegian Caledonides: Implications for the development of Iapetus: Contributions to Mineralogy and Petrology, v. 98, p. 13–23, https://doi.org/10.1007/BF00371904.

Fedo, C.M., Sircombe, K.N., and Rainbird, R.H., 2003, Detrital Zircon Analysis of the Sedimentary Record: Reviews in Mineralogy and Geochemistry, v. 53, p. 277–303, https://doi.org/10.2113/0530277.

Finetti, I.R., Boccaletti, M., Bonini, M., Del Ben, A., Geletti, R., Pipan, M., and Sani, F., 2001, Crustal section based on CROP seismic data across the North Tyrrhenian-Northern Apennines: Adriatic Sea: Tectonophysics, v. 343, p. 135–163, https://doi.org/10.1016/S0040-1951(01)00141-X.

Foley, S.F., 1992, Petrological characterisation of the source components of potassic magmas: Geochemical and experimental constraints: Lithos, v. 28, p. 187–204, https://doi.org/10.1016/0024-4937(92)90006-K.

Foley, S.F., Venturelli, G., Green, D.H., and Toscani, L., 1987, The ultrapotassic rocks: Characteristics, classification, and constraints for petrogenetic models: Earth-Science Reviews, v. 24, p. 81–134, https://doi.org/10.1016/0012-8252(87)90001-8.

Furnes, H., Roberts, D., Sturt, B.A., Thon, A., and Gale, G.H., 1980, Ophiolite fragments in the Scandinavian Caledonides: Proceedings International Ophiolite Symposium, Nicosia, 1979, Cyprus Geological Survey Department, p. 582–600.

Furnes, H., Ryan, P.D., Grenne, T., Roberts, D., Sturt, B.A., and Prestvik, T., 1985, Geological and geochemical classification of the ophiolitic fragments in the Scandinavian Caledonides, in Gee, D.G., and Sturt, B.A., eds, The Caledonide Orogen: Scandinavia and Related Areas, Part 2: Chichester, UK, John Wiley & Sons Ltd., p. 657–669.

Furnes, H., Dilek, Y., and Pedersen, R.R., 2012, Structure, geochemistry, and tectonic evolution of a trench-distal backarc oceanic crust in the western Norwegian Caledonides, Solund-Stavfjord ophiolite (Norway): Geological Society of America Bulletin, v. 124, p. 1027–1047, https://doi.org/10.1130/B30561.1.

Furnes, H., de Wit, M., and Dilek, Y., 2014, Four billion years of ophiolites reveal secular trends in oceanic crust formation: Geoscience Frontiers, v. 5, p. 571–603, https://doi.org/10.1016/j.gsf.2014.02.002.

Gale, A., Dalton, C., Langmuir, C.H., Su, Y., and Schilling, J.G., 2013, The mean composition of ocean ridge basalts: Geochemistry, Geophysics, Geosystems, v. 14, p. 489–518, https://doi.org/10.1029/2012GC004334.

Gao, Y., Hou, Z., Kamber, B.S., Wei, R., Meng, X., and Zhao, R., 2007, Lamproitic rocks from a continental collision zone: Evidence for recycling of subducted Tethyan oceanic sediments in the mantle beneath southern Tibet: Journal of Petrology, v. 48, p. 729–752, https://doi.org/10.1093/petrology/egl080.

Gee, D.G., 1981, The Dictyonema-bearing phyllites at Nordaunevoll, eastern Trøndelag, Norway: Norsk Geologisk Tidsskrift, v. 61, p. 93–95.

Gee, D.G., Guezou, J.C., Roberts, D., and Wolff, F.C., 1985, The central-southern part of the Scandinavian Caledonides, in Gee, D.G., and Sturt, B.A., eds, The Caledonide Orogen: Scandinavia and Related Areas, Part 1: Chichester, UK, John Wiley & Sons Ltd., p. 109–133.

Giampaolo, C., Godano, R.F., Di Sabatino, B., and Barrese, E., 1997, The alteration of leucite-bearing rocks: A possible mechanism: European Journal of Mineralogy, v. 9, p. 1293–1310, https://doi.org/10.1127/ejm/9/6/1277.

Gjelle, S., and Sigmond, E.M.O., 1995, Bergartsklassifikasjon og kartfremstilling: Geological Survey of Norway Skrifter, v. 113, 85 p.

Grenne, T., 1980, Vassfjellet area, in Wolff, F.C., ed., Excursions Across Part of the Trondheim Region, Central Norwegian Caledonides: Geological Survey of Norway Bulletin, v. 356, p. 159–164.

Grenne, T., 1989, Magmatic evolution of the Løkken SSZ Ophiolite, Norwegian Caledonides: Relationships between anomalous lavas and high-level intrusions: Geological Journal, v. 24, p. 251–274, https://doi.org/10.1002/gj.3350240403.

Grenne, T., and Roberts, D., 1983, Volcanostratigraphy and eruptive products of the Jonsvatn Greenstone Formation: Central Norwegian Caledonides: Geological Survey of Norway Bulletin, v. 387, p. 21–38.

Grenne, T., and Roberts, D., 1998, The Hølonda Porphyrites, Norwegian Caledonides: Geochemistry and tectonic setting of Early–Mid-Ordovician shoshonitic volcanism: Journal of the Geological Society, v. 155, p. 131–142, https://doi.org/10.1144/gsjgs.155.1.0131.

Grenne, T., and Slack, J.F., 2019, Mineralogy and geochemistry of silicate, sulfide, and oxide iron formations in Norway: Evidence for fluctuating redox states of early Paleozoic marine basins: Mineralium Deposita, v. 54, p. 829–848, https://doi.org/10.1007/s00126-018-0840-2.

Grenne, T., Grammeltvedt, G., and Vokes, F.M., 1980, Cyprus-type sulphide deposits in the western Trondheim district, central Norwegian Caledonides: Proceedings International Ophiolite Symposium, Nicosia, 1979, Cyprus Geological Survey Department, p. 727–743.

Grenne, T., Ihlen, P., and Vokes, M., 1999, Scandinavian Caledonide Metallogeny in a plate tectonic perspective: Mineralium Deposita, v. 34, p. 422–471, https://doi.org/10.1007/s001260050215.

Guo, Z., Wilson, M., Zhang, M., Cheng, Z., and Zhang, L., 2015, Post-collisional ultrapotassic mafic magmatism in South Tibet: Products of partial melting of pyroxenite in the mantle wedge induced by roll-back and delamination of the subducted Indian continental lithosphere slab: Journal of Petrology, v. 56, p. 1365–1406, https://doi.org/10.1093/petrology/egv040.

Harland, W.B., and Gayer, R.A., 1972, The Arctic Caledonides and earlier oceans: Geological Magazine, v. 109, p. 289–314, https://doi.org/10.1017/S0016756800037717.

Harper, D.A.T., Mac Niocaill, C., and Williams, S.H., 1996, The palaeogeography of early Ordovician Iapetus terranes: An integration of faunal and palaeomagnetic constraints: Palaeogeography, Palaeoclimatology, Palaeoecology, v. 121, p. 297–312, https://doi.org/10.1016/0031-0182(95)00079-8.

Hastie, A.R., Kerr, A.C., Pearce, J.A., and Mitchell, S.F., 2007, Classification of altered volcanic island arc rocks using immobile trace elements: Development of the Th-Co discrimination diagram: Journal of Petrology, v. 48, p. 2341–2357, https://doi.org/10.1093/petrology/egm062.

Heim, M., Grenne, T., and Prestvik, T., 1987, The Resfjell ophiolite fragment, southwest Trondheim region, central Norwegian Caledonides: Geological Survey of Norway Bulletin, v. 409, p. 49–71.

Hollis, S.P., Roberts, S., Cooper, M.R., Earl, G., Herrington, R., and Condon, D.J., 2012, Episodic arc-ophiolite emplacement and the growth of continental margins: Late accretion in the Northern Irish sector of the Grampian-Taconic orogeny: Geological Society of America Bulletin, v. 124, p. 1702–1723, https://doi.org/10.1130/B30619.1.

Hollocher, K., Robinson, P., Seaman, K., and Walsh, E., 2016, Ordovician-early Silurian intrusive rocks in the Northwest part of the Upper Allochthon, mid-Norway: Plutons of an Iapetan volcanic arc complex: American Journal of Science, v. 316, p. 925–980, https://doi.org/10.2475/10.2016.01.

Hulsbosch, N., 2019, Nb-Ta-Sn-W distribution in granite-related ore systems, in Decrée, S., and Robb, L., eds., Ore Deposits: Origin, Exploration, and Exploitation: American Geophysical Union, Geophysical Monograph Series, v. 242, p. 75–107, https://doi.org/10.1002/9781119290544.ch4.

Kessel, L., and Busby, C.J., 2003, Analysis of VHMS-hosting ignimbrites erupted at bathyal water depths (Ordovician Bald Mountain sequence, northern Maine), in White, J.D.L., Smellie, J.L., and Clague, D.A., eds., Explosive Subaqueous Volcanism: American Geophysical Union, Geophysical Monograph Series, v. 140, p. 372–392, https://doi.org/10.1029/140GM24.

Kjerulf, T., 1883, Merakerprofilet: Det Kongelige Norske Videnskabers Selskabs: Trondhjem, Norway, Skrifter, 63 p.

Lehmann, B., 2021, Formation of tin ore deposits: A reassessment: Lithos, no. 105756, https://doi.org/10.1016/j.lithos.2020.105756.

Ludwig, K.R., 2003, User's Manual for Isoplot 3.00: A Geochronological Toolkit for Microsoft Excel: Berkeley Geochronology Center Special Publication, v. 4, 70 p.

Mantovani, E., Viti, M., Babbucci, D., Tamburelli, C., and Cenni, N., 2020, Geodynamics of the central-western Mediterranean region: Plausible and non-plausible driving forces: Marine and Petroleum Geology, v. 113, no. 104121, https://doi.org/10.1016/j.marpetgeo.2019.104121.

Mitchell, R.H., and Bergman, S.C., 1991, Petrology of Lamproites: New York and London, Plenum Press, 443 p., https://doi.org/10.1007/978-1-4615-3788-5.

Natland, J.H., 1980, Effect of axial magma chambers beneath spreading centers on the composition of basaltic rocks: Initial Reports of the Deep Sea Drilling Project, v. 54, p. 833–852, https://doi.org/10.2973/dsdp.proc.54.138.1980.

Neuman, R.B., and Bruton, D.L., 1989, Brachiopods and trilobites from the Ordovician Lower Hovin Group (Arenig/Llanvirn), Hølonda area, Trondheim Region, Norway: New and revised taxa and paleogeographic interpretation: Geological Survey of Norway Bulletin, v. 414, p. 49–89.

Nilsen, O., and Wolff, F.C., 1989, Bedrock map Røros og Sveg M 1:250000: Geological Survey of Norway.

Niu, Y., and O'Hara, M.J., 2003, Origin of ocean island basalts: A new perspective from petrology, geochemistry, and mineral physics considerations: Journal of Geophysical Research. Solid Earth, v. 108, no. 2209, https://doi.org/10.1029/2002JB002048.

Niu, Y., and O'Hara, M.J., 2008, Global correlations of ocean ridge basalt chemistry with axial depth: A new perspective: Journal of Petrology, v. 49, p. 633–664, https://doi.org/10.1093/petrology/egm051.

Niu, Y., Bideau, D., Hekinian, R., and Batiza, R., 2001, Mantle compositional control on the extent of melting, crust production, gravity anomaly and ridge morphology: A case study at the Mid-Atlantic Ridge 33–35°N: Earth and Planetary Science Letters, v. 186, p. 383–399, https://doi.org/10.1016/S0012-821X(01)00255-2.

Pearce, J.A., 1996, A user's guide to basalt discrimination diagrams: Geological Association of Canada, Short Course Notes, v. 12, p. 79–113.

Pearce, J.A., 2014, Immobile element fingerprinting of ophiolites: Elements, v. 10, p. 101–108, https://doi.org/10.2113/gselements.10.2.101.

Pearce, J.A., and Peate, D.W., 1995, Tectonic implications of the composition of volcanic arc magmas: Annual Review of Earth and Planetary Sciences, v. 23, p. 251–285, https://doi.org/10.1146/annurev.ea.23.050195.001343.

Pearce, J.A., and Stern, R.J., 2006, Origin of back-arc basin magmas: Trace element and isotope perspectives,

in Christie, D.M., Fisher, C.R., Lee, S.M., Givens, S., eds., Back-Arc Spreading Systems: Geological, Biological, Chemical, and Physical Interactions: Geophysical Monograph Series, v. 166, p. 63–86, https://doi.org/10.1029/166GM06.

Peccerillo, A., 1999, Multiple mantle metasomatism in central-southern Italy: Geochemical effects, timing and geodynamic implications: Geology, v. 27, p. 315–318, https://doi.org/10.1130/0091-7613(1999)027<0315:MMMICS>2.3.CO;2.

Peccerillo, A., 2005, Plio-Quaternary Volcanism in Italy: Berlin, Heidelberg, Germany, Springer, 370 p., https://doi.org/10.1007/3-540-29092-3.

Pedersen, R.B., Bruton, D.L., and Furnes, H., 1992, Ordovician faunas, island arcs and ophiolites in the Scandinavian Caledonides: Terra Nova, v. 4, p. 217–222, https://doi.org/10.1111/j.1365-3121.1992.tb00475.x.

Perfit, M.R., 2001, Mid-ocean ridge geochemistry and petrology, *in* Steele, J.H., ed., Encyclopedia of Ocean Sciences: Cambridge, Massachusetts, USA, Academic Press, p. 1778–1788, https://doi.org/10.1006/rwos.2001.0096.

Pouclet, A., Lee, J.-S., Vidal, P., Cousens, B., and Bellon, H., 1995, Cretaceous to Cenozoic volcanism in South Korea and in the Sea of Japan: Magmatic constraints on the opening of the back-arc basin, *in* Smellie, J.L., ed., Volcanism Associated with Extension at Consuming Plate Margins: Geological Society of London, Special Publication, v. 81, p. 169–191, https://doi.org/10.1144/GSL.SP.1994.081.01.10.

Prelević, D., Foley, S.F., Cvetkovic, V., and Romer, R.L., 2004, The analcime problem and its impact on the geochemistry of ultrapotassic rocks from Serbia: Mineralogical Magazine, v. 68, p. 633–648, https://doi.org/10.1180/0026461046840209.

Prelević, D., Foley, S.F., Romer, R., and Conticelli, S., 2008, Mediterranean Tertiary lamproites derived from multiple source components in postcollisional geodynamics: Geochimica et Cosmochimica Acta, v. 72, p. 2125–2156, https://doi.org/10.1016/j.gca.2008.01.029.

Rainbird, R.H., Hamilton, M.A., and Young, G.M., 2001, Detrital zircon geochronology and provenance of the Torridonian, NW Scotland: Journal of the Geological Society, v. 158, p. 15–27, https://doi.org/10.1144/jgs.158.1.15.

Roberts, D., and Wolff, F., 1981, Tectonostratigraphic development of the Trondheim region Caledonides, central Norway: Journal of Structural Geology, v. 3, p. 487–494, https://doi.org/10.1016/0191-8141(81)90048-1.

Roberts, D., Grenne, T., and Ryan, P.D., 1984, Ordovician marginal basin development in the central Norwegian Caledonides: Geological Society of London, Special Publications, v. 16, p. 233–244, https://doi.org/10.1144/GSL.SP.1984.016.01.18.

Roberts, D., Sturt, B.A., and Furnes, H., 1985, Volcanite assemblages and environments in the Scandinavian Caledonides and the sequential development history of the mountain belt, *in* Gee, D.G., and Sturt, B.A., eds, The Caledonide Orogen: Scandinavia and related areas, Part 2: Chichester, UK, John Wiley & Sons Ltd., p. 919–930.

Roberts, D., Walker, N., Slagstad, T., Solli, A., and Krill, A., 2002, U-Pb zircon ages from the Bymarka ophiolite, near Trondheim, central Norwegian Caledonides, and regional implications: Norsk Geologisk Tidsskrift, v. 82, p. 19–30.

Rogers, N., and van Staal, C.R., 2003, Volcanology and tectonic setting of the northern Bathurst Mining Camp: Part II. Mafic volcanic constraints on back-arc opening, *in* Goodfellow, W.D., McCutcheon, S.R., and Peter, J.M., eds, Massive Sulphide Deposits of the Bathurst Mining Camp, New Brunswick, and Northern Maine: Economic Geology Monograph, v. 11, p. 181–202.

Rosenbaum, G., 2014, Geodynamics of oroclinal bending: Insights from the Mediterranean: Journal of Geodynamics, v. 82, p. 5–15, https://doi.org/10.1016/j.jog.2014.05.002.

Royden, L.H., 1993, Evolution of retreating subduction boundaries formed during continental collision: Tectonics, v. 12, p. 629–638, https://doi.org/10.1029/92TC02641.

Rubin, K.H., Sinton, J.M., Maclennan, J., and Hellebrand, E., 2009, Magmatic filtering of mantle compositions at mid-ocean-ridge volcanoes: Nature Geoscience, v. 2, p. 321–328, https://doi.org/10.1038/ngeo504.

Rudnick, R.L., and Gao, S., 2003, Composition of the Continental Crust, *in* Holland, H.D., and Turekian, K.K., eds., Treatise on Geochemistry, v. 3, p. 1–64, https://doi.org/10.1016/B0-08-043751-6/03016-4.

Ryan, J.G., 2002, Trace element characteristics of beryllium in terrestrial materials: Reviews in Mineralogy and Geochemistry, v. 50, p. 121–145, https://doi.org/10.2138/rmg.2002.50.3.

Ryan, P.D., and Dewey, J.F., 1991, A geological and tectonic cross-section of the Caledonides of western Ireland: Journal of the Geological Society, v. 148, p. 173–180, https://doi.org/10.1144/gsjgs.148.1.0173.

Ryan, P.D., and Dewey, J.F., 2011, Arc-continent collision in the Ordovician of western Ireland: Stratigraphic, structural and metamorphic evolution, *in* Brown, D., and Ryan, P.D., eds., Arc-Continent Collision: Frontiers in Earth Sciences: Berlin, Heidelberg, Germany, Springer, p. 373–401, https://doi.org/10.1007/978-3-540-88558-0_13.

Saccani, E., 2015, A new method of discriminating different types of post-Archean ophiolitic basalts and their tectonic significance using Th-Nb and Ce-Dy-Yb systematics: Geoscience Frontiers, v. 6, p. 481–501, https://doi.org/10.1016/j.gsf.2014.03.006.

Saccani, E., Principi, G., Garfagnoli, F., and Menna, F., 2008, Corsica ophiolites: Geochemistry and petrogenesis of basaltic and metabasaltic rocks: Ofioliti, v. 33, p. 187–207, https://doi.org/10.4454/OFIOLITI.V33I2.369.

Seilacher, A., 1967, Bathymetry of trace fossils: Marine Geology, v. 5, p. 413–428, https://doi.org/10.1016/0025-3227(67)90051-5.

Shinjo, R., Chung, S.L., Kato, Y., and Kimura, M., 1999, Geochemical and Sr-Nd isotopic characteristics of volcanic rocks from the Okinawa Trough and Ryukyu Arc: Implications for the evolution of a young, intra-ontinental back arc basin: Journal of Geophysical Research. Solid Earth, v. 104, p. 10591–10608, https://doi.org/10.1029/1999JB900040.

Slagstad, T., 2003, Geochemistry of trondhjemites and mafic rocks in the Bymarka ophiolite fragment, Trondheim, Norway: Petrogenesis and tectonic implications: Norsk Geologisk Tidsskrift, v. 83, p. 167–185.

Slagstad, T., and Kirkland, C.L., 2017, The use of detrital zircon data in terrane analysis: A nonunique answer to provenance and tectonostratigraphic position in the Scandinavian Caledonides: Lithosphere, v. 9, p. 1002–1011, https://doi.org/10.1130/L663.1.

Slagstad, T., Pin, C., Roberts, D., Kirkland, C., Grenne, T., Dunning, G., Sauer, S., and Andersen, T., 2014, Tectonomagmatic evolution of the Early Ordovician suprasubduction-zone ophiolites of the Trondheim Region, Mid-Norwegian Caledonides, *in* Corfu, F., Gasser, D., and Chew, D., eds., New Perspectives on the Caledonides of Scandinavia and related Areas: Geological Society of London, Special Publication, v. 390, p. 541–561, https://doi.org/10.1144/SP390.11.

Smelror, M., Solbakk, T., Rindstad, B.I., Stuedal, H.V., and Hårsaker, K., 2020, Notes on Ordovician graptolites, nautiloids and trace fossils from Lånke, Central Norwegian Caledonides: Norsk Geologisk Tidsskrift, v. 100, no. 202007, https://doi.org/10.17850/njg100-2-2.

Spencer, C.J., and Kirkland, C.L., 2016, Visualizing the sedimentary response through the orogenic cycle: A multidimensional scaling approach: Lithosphere, v. 8, p. 29–37, https://doi.org/10.1130/L479.1.

Stern, R.J., and Gerya, T., 2018, Subduction initiation in nature and models: A review: Tectonophysics, v. 746, p. 173–198, https://doi.org/10.1016/j.tecto.2017.10.014.

Stokke, E.W., Gasser, D., Dalsååen, B.H., and Grenne, T., 2018, Tectonic evolution of syn-to late-orogenic sedimentary-volcanic basins in the central Norwegian Caledonides: Journal of the Geological Society, v. 175, p. 605–618, https://doi.org/10.1144/jgs2017-091.

Sturt, B.A., Roberts, D., and Furnes, H., 1984, A conspectus of Scandinavian Caledonian ophiolites, *in* Gass, I.G., Lippard, S.J., and Shelton, A.W., eds., Ophiolites and Oceanic Lithosphere: Geological Society of London, Special Publication, v. 13, p. 381–391, https://doi.org/10.1144/GSL.SP.1984.013.01.31.

Sun, S., and McDonough, W.F., 1989, Chemical and isotopic systematics of oceanic basalts: Implications for mantle composition and processes, *in* Saunders, A.D., and Morry, M.J., eds., Magmatism in the Ocean Basins: Geological Society of London, Special Publication, v. 42, p. 313–345, https://doi.org/10.1144/GSL.SP.1989.042.01.19.

Teng, L.S., 1990, Geotectonic evolution of late Cenozoic arc-continent collision in Taiwan: Tectonophysics, v. 183, p. 57–76, https://doi.org/10.1016/0040-1951(90)90188-E.

Teng, L.S., 1996, Extensional collapse of the northern Taiwan mountain belt: Geology, v. 24, p. 949–952, https://doi.org/10.1130/0091-7613(1996)024<0949:ECOTNT>2.3.CO;2.

van Staal, C.R., Winchester, J.A., and Bedard, J.H., 1991, Geochemical variations in Middle Ordovician volcanic rocks of the northern Miramichi Highlands and their tectonic significance: Canadian Journal of Earth Sciences, v. 28, p. 1031–1049, https://doi.org/10.1139/e91-094.

van Staal, C.R., Whalen, J.B., Valverde-Vaquero, P., Zagorevski, A., and Rogers, N., 2009, Pre-Carboniferous, episodic accretion-related, orogenesis along the Laurentian margin of the northern Appalachians, *in* Murphy, J.B., Keppie, J.D., and Hynes, A.J., eds., Ancient Orogens and Modern Analogues: Geological Society of London, Special Publication, v. 327, p. 271–316, https://doi.org/10.1144/SP327.13.

Veizer, J., Ala, D., Azmy, K., Bruckschen, P., Buhl, D., Bruhn, F., Carden, G.A.F., Diener, A., Ebneth, S., Godderis, Y., Jasper, T., Korte, C., Pawellek, F., Podlaha, O.G., and Strauss, H., 1999, $^{87}Sr/^{86}Sr$, $\delta^{13}C$ and $\delta^{18}O$ evolution of Phanerozoic seawater: Chemical Geology, v. 161, p. 59–88, https://doi.org/10.1016/S0009-2541(99)00081-9.

Vignaroli, G., Faccenna, C., Jolivet, L., Piromallo, C., and Rossetti, F., 2008, Subduction polarity reversal at the junction between the Western Alps and the Northern Apennines, Italy: Tectonophysics, v. 450, p. 34–50, https://doi.org/10.1016/j.tecto.2007.12.012.

Wallace, P.J., 2005, Volatiles in subduction zone magmas: Concentrations and fluxes based on melt inclusion and volcanic gas data: Journal of Volcanology and Geothermal Research, v. 140, p. 217–240, https://doi.org/10.1016/j.jvolgeores.2004.07.023.

Walsh, J.J., 1986, The Geology of the Caledonian Rocks of SE Meldal, Sør-Trøndelag, Norway [Ph.D. thesis]: Galway, Ireland, University College Galway, 307 p.

Wang, K.L., Chung, S.L., Chen, C.H., Shinjo, R., Yang, T.F., and Chen, C.H., 1999, Post-collisional magmatism around northern Taiwan and its relation with opening of the Okinawa Trough: Tectonophysics, v. 208, p. 363–376, https://doi.org/10.1016/S0040-1951(99)00111-0.

Wang, K.L., Chung, S.L., O'Reilly, S.Y., Sun, S.S., Shinjo, R., and Chen, Ch.H., 2004, Geochemical constraints for the genesis of post-collisional magmatism and the geodynamic evolution of the northern Taiwan Region: Journal of Petrology, v. 45, p. 975–1011, https://doi.org/10.1093/petrology/egh001.

Waters, C.L., Sims, K.W.W., Perfit, M.R., Blichert-Toft, J., and Blusztajn, J., 2011, Perspective on the Genesis of E-MORB from Chemical and Isotopic Heterogeneity at 9–10°N East Pacific Rise: Journal of Petrology, v. 52, p. 565–602, https://doi.org/10.1093/petrology/egq091.

White, W.M., and Klein, E.M., 2014, Composition of the oceanic crust, *in* Holland, H.D., and Turekian, K.K., eds., Treatise on Geochemistry (Second Edition), v. 4, p. 457–496, http://dx.doi.org/10.1016/B978-0-08-095975-7.00315-6.

Wilson, J.T., 1966, Did the Atlantic close and then re-open?: Nature, v. 211, p. 676–681, https://doi.org/10.1038/211676a0.

Wolff, F.C., 1976, Bedrock map Trondheim: Geological Survey of Norway, scale 1:250,000.

Wolff, F.Ch., 1979, Beskrivelse til de berggrunnsgeologiske kart Trondheim og Østersund 1:250 000 (med fargetrykt kart): Geological Survey of Norway Skrifter, v. 353, p. 1–76.

Wood, B.J., Kiseeva, E.S., and Matzen, A., 2013, Garnet in the Earth's mantle: Elements, v. 9, p. 421–426, https://doi.org/10.2113/gselements.9.6.421.

Zagorevski, A., and van Staal, C.R., 2011, The record of Ordovician Arc-Arc and Arc-Continent collisions in the Canadian Appalachians during the closure of Iapetus, *in* Brown, D., and Ryan, P.D., eds., Arc-Continent Collision: Frontiers in Earth Sciences, p. 341–371, https://doi.org/10.1007/978-3-540-88558-0_12.

Zagorevski, A., Rogers, N., van Staal, C.R., McNicoll, V., Lissenberg, C.J., and Valverde-Vaquero, P., 2006, Lower to Middle Ordovician evolution of peri-Laurentian arc and backarc complexes in Iapetus: Constraints from the Annieopsquotch accretionary tract, central Newfoundland: Geological Society of America Bulletin, v. 118, p. 324–342, https://doi.org/10.1130/B25775.1.

Zagorevski, A., Lissenberg, C.J., and van Staal, C.R., 2009, Dynamics of accretion of arc and backarc crust to continental margins: Inferences from the Annieopsquotch accretionary tract, Newfoundland Appalachians: Tectonophysics, v. 479, p. 150–164, https://doi.org/10.1016/j.tecto.2008.12.002.

Zhao, Z., Xiong, X., Wang, Q., Bai, Z., and Qiao, Y., 2009, Late Paleozoic underplating in North Xinjiang: Evidence from shoshonites and adakites: Gondwana Research, v. 16, p. 216–226, https://doi.org/10.1016/j.gr.2009.03.001.

Zhou, X., Li, Z.H., Gerya, T.V., and Stern, R.J., 2020, Lateral propagation–induced subduction initiation at passive continental margins controlled by preexisting lithospheric weakness: Science Advances, v. 6, no. 10, https://doi.org/10.1126/sciadv.aaz1048.